A CMOS Biosensor for Infectious Disease Detection

Turgut Sefket Aytur

Electrical Engineering and Computer Sciences
University of California at Berkeley

Technical Report No. UCB/EECS-2007-108
http://www.eecs.berkeley.edu/Pubs/TechRpts/2007/EECS-2007-108.html

August 24, 2007

Acknowledgement

I would like to thank my advisor, Professor Bernhard Boser, for his support and guidance; Professors Eva Harris and P. Robert Beatty, for their support, enthusiasm, and encouragement; Jonathan Foley, for conducting experiments and numerous constructive discussions; Tomohiro Ishikawa, for fabricating hardware and providing diplomacy; the research group of Professor Eva Harris, for support and understanding toward engineers with misconceptions about biology; and the Acumen Foundation, for financial support.

A CMOS Biosensor for Infectious Disease Detection

by

Turgut Sefket Aytür

B.Sc. (Princeton University) 1993

M.Sc. (Columbia University) 1996

A dissertation submitted in partial satisfaction of

the requirements for the degree of

Doctor of Philosophy

in

Engineering - Electrical Engineering and Computer Sciences

in the

GRADUATE DIVISION

of the

UNIVERSITY OF CALIFORNIA, BERKELEY

Committee in charge:

Professor Bernhard E. Boser, Chair

Professor Kristopher S. J. Pister

Professor Eva Harris

Fall 2007

The dissertation of Turgut Sefket Aytür is approved:

_____

Chair Date

_____

Date

_____

Date

A CMOS Biosensor for Infectious Disease Detection

by

Turgut Sefket Aytür

To my parents.

Contents

Chapter 1: Introduction 1

1.1 The Enzyme-Linked Immunosorbent Assay (ELISA) 2

1.2 Paramagnetic Microparticles 4

1.3 Magnetic-Particle Assay 4

1.4 Magnetic-Sensor Technology 7

Chapter 2: Sensor Design and System Architecture 9

2.1 Technological Challenges 9

2.2 Magnetic-Bead Signal 9

2.2.1 Magnetic-Field Calculation 9

2.2.2 Magnetic-Field Simulation 10

2.2.3 Dynamic Effects 13

2.3 CMOS Magnetic-Sensor Design 14

2.3.1 Topology Selection 14

2.3.2 Sensor Design Parameters 16

2.3.3 Sensor Noise 18

2.4 System Design 19

2.4.1 Sensor-Chip Architecture 19

2.4.2 Electrical Modulation 21

2.5 Sensor-Chip Fabrication 22

2.5.1 CMOS Processing 22

2.5.2 Post-Processing 23

2.6 Fluidic Packaging and Module Assembly 27

2.7 Measurement System 30

2.7.1 Reader Hardware 30

2.7.2 Magnetic Washing 32

2.8 Software and Calibration Algorithms 34

2.8.1 Error Sources and Calibration 34

2.8.2 Software Design 35
2.8.3 System Performance 36
2.9 Design Summary 38
Chapter 3: Magnetic-Particle Assay (MPA) Platform Evaluation 40
3.1 Methodology 40
3.2 Purified-Protein Assays 41
3.2.1 ELISA 41
3.2.2 Magnetic-Particle Assay (MPA) 44
3.2.3 Platform Comparison 47
3.3 Serum Assay for the Detection of Dengue Virus 49
3.3.1 Background 49
3.3.2 ELISA 51
3.3.3 Magnetic-Particle Assay (MPA) 52
3.3.4 Platform Comparison 54
3.4 Assessment 56
3.4.1 Magnetic-Particle Assay (MPA) Protocol and Correlation 56
3.4.2 Magnetic Bead Selection 57
3.4.3 Magnetic Washing 59
Chapter 4: Overall Platform Assessment 61
4.1 CMOS Sensor 61
4.2 Application Benefits 62
4.3 Clinical Validity 64
4.4 Next Steps 65
Bibliography 67
Appendix 70
Appendix A: Post-Processing Steps 70
Appendix B: Matlab Code 71
Appendix C: Purified-Protein ELISA Protocol 80
Appendix D: Purified-Protein MPA Protocol 81
Appendix E: Serum ELISA Protocol 82
Appendix F: Serum MPA Protocol 83

Acknowledgements

I would like to thank my advisor, Professor Bernhard Boser, for his support and guidance; Professors Eva Harris and P. Robert Beatty, for their support, enthusiasm, and encouragement; Jonathan Foley, for conducting experiments and numerous constructive discussions; Tomohiro Ishikawa, for fabricating hardware and providing diplomacy; the research group of Professor Eva Harris, for support and understanding toward engineers with misconceptions about biology; and the Acumen Foundation, for financial support.

Chapter 1

Introduction

The timely and accurate diagnosis of infectious diseases is indispensable for directing patient management and informing larger public health decisions. For the individual patient, delays in accurate diagnosis may delay necessary treatment and consequently result in a negative outcome. From the public health standpoint, prompt awareness of disease outbreaks is critical for an effective response. In developed countries, both the medical infrastructure and the public health service departments have significant resources aligned to the detection and prevention of infectious disease. Hospitals have large laboratory facilities capable of testing thousand of patient samples per day. In addition, the density of medical facilities is high enough that access to most detection technology is almost universal. In developing countries, these resources are typically much less available. Large fractions of their populations do not have access to modern hospitals and diagnostic services and equipment, relying instead on small clinics and point-of-care diagnostics. It is in this setting that most diagnostic technologies designed and deployed in developed countries fail (Mabey et al., 2004). To be successful in this environment, major improvements in cost, portability, and ease-of-use are required. This objective has been met in some qualitative assays, where "yes" or "no" outcomes are clinically sufficient. However, quantitative results are often essential in both diagnosis and treatment of many diseases. With this requirement, current diagnostic systems are costly, complex, and too large for point-of-care applications. A new approach is required to meet this need.

1.1 The Enzyme-Linked Immunosorbent Assay (ELISA)

Enzyme-linked Immunosorbent Assays (ELISAs) in various forms are the predominant immunological diagnostic assays used in most clinical settings. This assay relies on the antibody-ligand binding behavior that characterizes antibody action in an immune response.

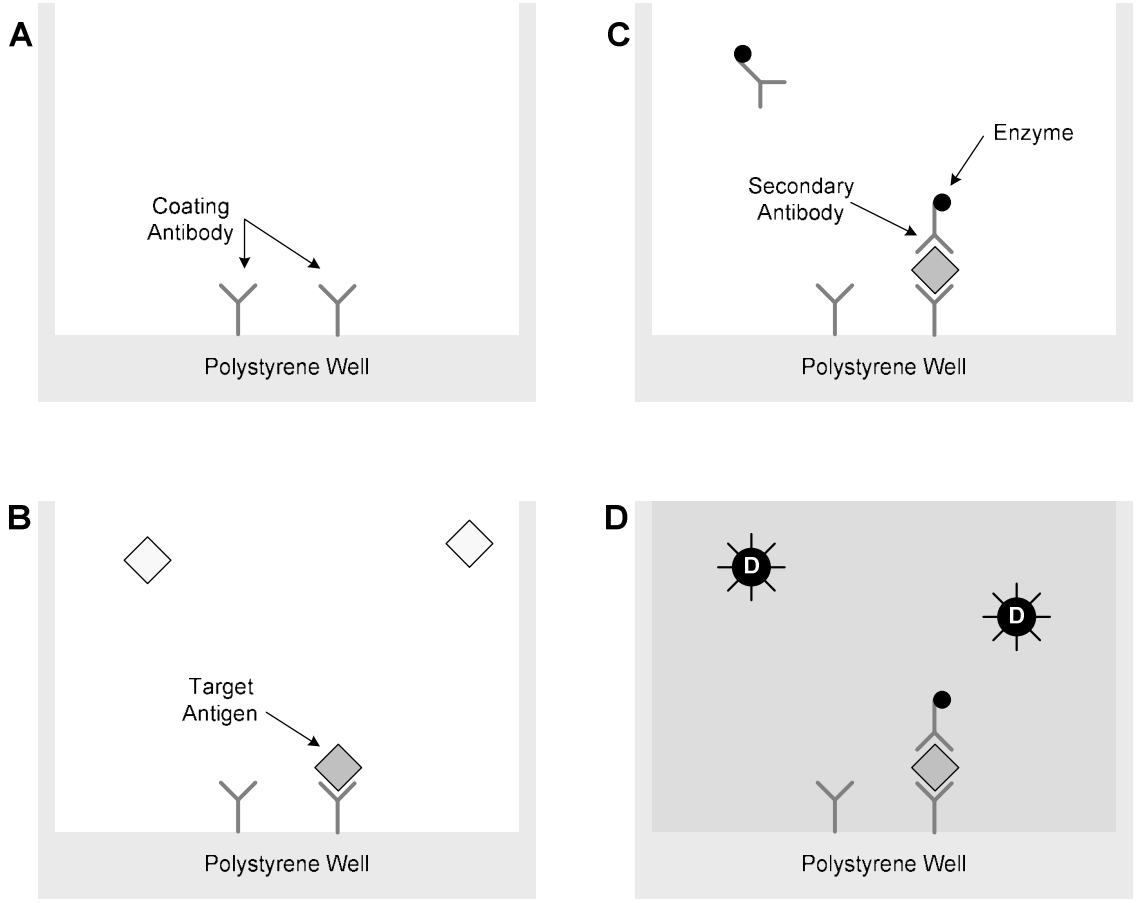

Figure 1.1: Simplified representation of an Enzyme-Linked Immunosorbent Assay (ELISA), including antibody coating (A), antigen binding (B), enzyme-linked secondary antibody (C), and substrate-dye catalysis (D).

An example of the ELISA protocol is shown in Figure 1.1. First, polystyrene wells are coated with a protein that binds specifically to the target. Polystyrene efficiently adsorbs proteins, and they remain attached to this surface and functional even if the sample well is washed repeatedly. Figure 1.1A shows an antibody used as a coating protein, and it binds only to the specific antigen shown in Figure 1.1B. This type of ELISA is commonly referred to as an antigen-capture format, but many other configurations are possible. Next, a secondary protein is added that is also specific to the target antigen (Figure 1.1C). This antibody is conjugated with an enzyme that catalyzes the dye in (Figure 1.1D). After a certain time, the presence of the target antigen is indirectly indicated by a color change in the liquid. The amount of color change is a function of the amount of enzyme present, and the amount of time that the enzyme is allowed to catalyze the dye reaction. To accurately quantify the concentration of the analyte, a spectrophotometer is used.

Typical ELISAs perform sufficiently to address a broad range of both qualitative and quantitative needs; however, the ELISA platform requires laboratory facilities and equipment that are restrictive for point-of-care diagnostics. Specifically, standard ELISAs require numerous liquid washing steps and quantitation that depends on a spectrophotometer that is not available in a mobile, battery-powered form. The priorities for point-of-care diagnostics are rapidity, ease-of-use, and low cost while maintaining required clinical sensitivity. To achieve this, some intrinsic limitations of the ELISA format, such as quantitative color measurement, must be removed. Other features, such as broad applicability to different targets, should be preserved.

1.2 Paramagnetic Microparticles

Paramagnetic microparticles ("beads") are a valuable tool being applied to various analytical applications from imaging to drug delivery (Gijs, 2004). Paramagnetic beads differ from ferromagnetic objects in that they display little or no intrinsic magnetization. For simplicity, the term "paramagnetic beads" will be shortened to "magnetic beads" for the remainder of the text. Most beads are constructed of small (~10 nm) magnetite or maghemite particles that are suspended in a solid sphere of non-magnetic material. Numerous properties of magnetic beads make them suitable for widespread use: ease of manufacturing, manipulation in fluid, and a wide range of commercially available bead diameters, ranging from nanoparticles (50 nm) to microparticles (up to 20 μm). Smaller (50 nm) magnetic beads have long been used in research immunology for cell separation. Larger (1-5 μm) magnetic beads conjugated with antibodies have been utilized to separate target analytes in order to improve the performance of ELISAs by enhancing sensitivity and shortening incubation times (Gundersen et al., 1992, Gehring et al., 2004). In this format, the magnetic beads provide a larger surface area for capturing target molecules and facilitate manipulation; nonetheless, these immunoassay techniques do not utilize a sensor for detection of the magnetic beads and are limited by their reliance on spectrophotometers for optical detection.

1.3 Magnetic-Particle Assay (MPA)

The use of magnetic beads as a signal, with the incorporation of a magnetic-sensing mechanism, results in a Magnetic-Particle Assay (MPA). The assay concept is shown in Figure 1.2. Magnetic beads are coated with biologically active molecules (e.g.

antibodies), so that they become attached to the sensor surface when their complementary target analyte is present. The biochemistry shown in Figure 1.2 resembles the antigen-capture type ELISA in Figure 1.1, with antibodies bound to the sensor and magnetic bead surfaces. The sensor detects the magnetic field of the bead, indirectly indicating the presence of the analyte.

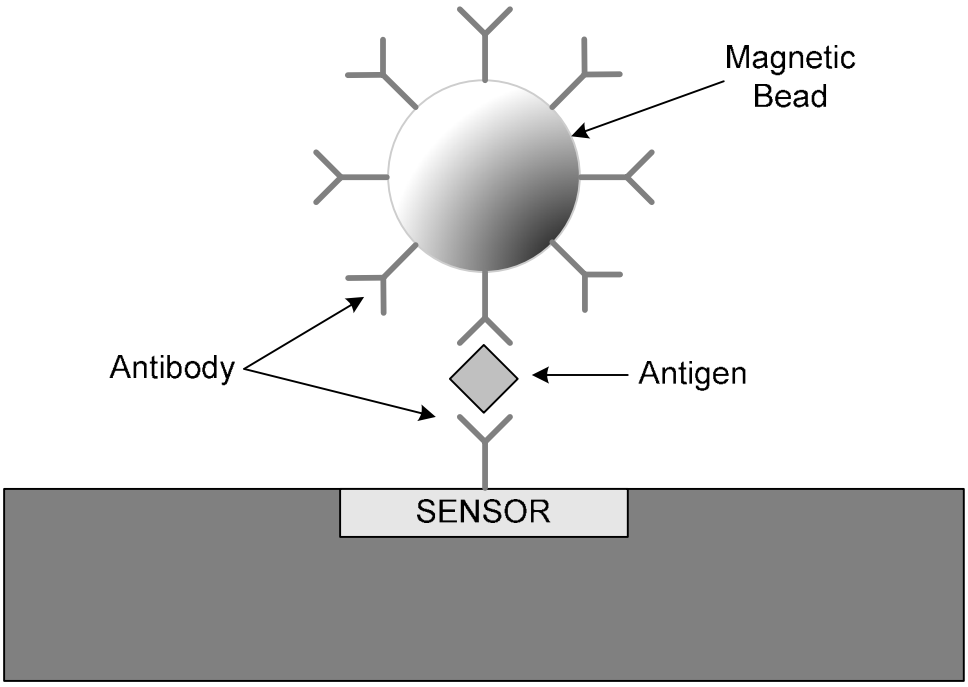

Figure 1.2: Magnetic-Particle Assay (MPA) concept, consisting of a magnetic bead, antibody-antigen binding, and a magnetic sensor.

Magnetic particle labels provide an advantage over traditional optical detection methods because they allow for the possibility of an optically opaque sample, as well as automated removal of non-specifically bound beads via a controlled magnetic field also known as "magnetic washing" (Baselt et al., 1998). This concept is shown in Figure 1.3.

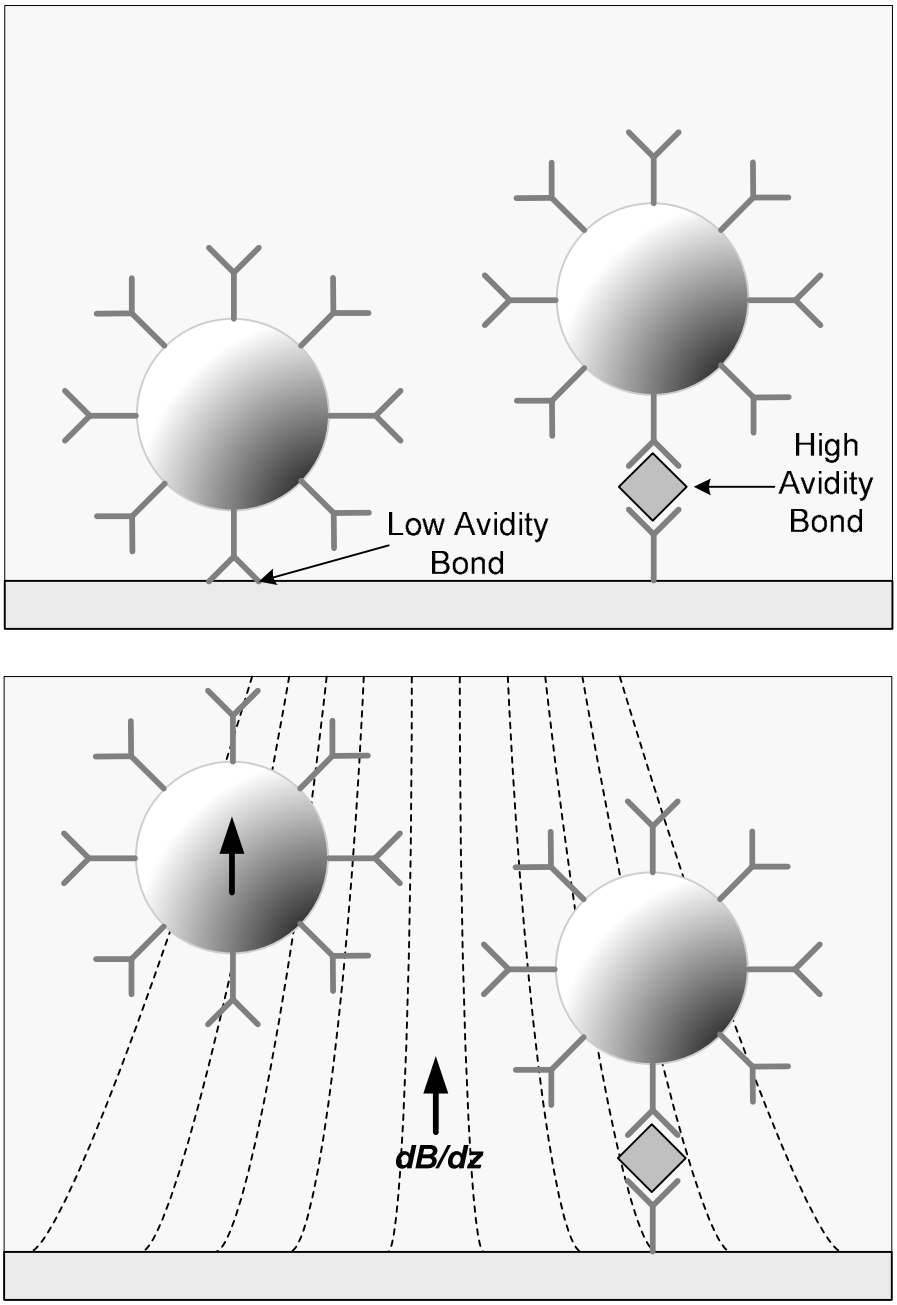

Figure 1.3: Magnetic washing concept, where nonspecifically-bound beads are pulled from the service a magnetic force, leaving specific bonds intact.

When an appropriate magnetic field gradient is applied to the beads, an upward force pulls nonspecifically bound beads (left) from the surface. These beads have lower

binding avidity than specifically bound beads (right), where strong ligand-receptor binding is involved. Magnetic washing has recently been demonstrated in immunoassays where the specific antigen binding of antibody-coated magnetic beads was differentiated from the non-specific binding of beads on the basis of magnetic force (Lee et al., 2000). Therefore, magnetic bead detection with magnetic washing could provide the automation and compact system integration desirable in rapid point-of-care diagnostics.

1.4 Magnetic-Sensor Technology

Magnetic sensors have been developed for the detection of magnetic beads in biological assays based on various technologies including giant magnetoresistive (GMR) sensors (Baselt et al., 1998, Kurlyandskaya et al., 2005, Rife et. al., 2003) and superconducting quantum interference devices (SQUID) (Chemla et al., 2000). Though SQUID sensors have very high sensitivity and low noise, they are not compact and the temperature requirements of the superconducting material make their use in point-of-care applications impractical. GMR-based sensors have good sensitivity and have been built into compact diagnostic modules. However, they are constructed using materials and fabrication processes infrequently used in the electronics industry, and hence do not leverage the economy-of-scale of more common technology. Recently, some evidence for the feasibility of CMOS technology in bead detection has been described (Besse et al., 2002). However, this approach has not been applied to biological assays.

Integrated circuits implemented in CMOS technology allow for the inclusion of laboratory functions and data processing within the sensor chip, enabling portability, reducing cost, and improving versatility. Computer chips have doubled in complexity

and functionality every 18 months for the last three decades, a trend commonly referred to as Moore's Law. CMOS, the technology underlying this progress, has demonstrated flexibility and gained wide industrial acceptance. CMOS-based devices are well suited for portable use due to their potential for integrating electronic functions of laboratory equipment in a compact form-factor at comparatively lower cost, which permits disposability. For example, CMOS technology has recently been used to create a compact and portable immunosensor for sensitive detection of bacteria (Song et al., 2005). However, this technology requires laser-induced fluorescence and is neither low-cost nor quantitative, therefore making it suboptimal for point-of-care diagnostic purposes.

In this work, a MPA platform targeted at infectious-disease detection is described. It is implemented using standard CMOS technology, in conjunction with limited post-processing. Chapter 2 examines the numerous challenges associated with implementing a magnetic sensor in CMOS with adequate performance for this application. The signal from a magnetic bead is estimated, and motivates both the sensor and the sensor chip architecture. In addition, software and calibration algorithms are described that compensate for manufacturing and implementation challenges. Chapter 3 compares the MPA protocol with ELISA in the context of two assays, with the goal of establishing clinical validity.

Chapter 2

Sensor Design and System Architecture

2.1 Technological Challenges

Though CMOS technology offers significant benefits in terms of economics and enables high integration levels, it also carries challenges in its performance as a magnetic field detector. Low carrier mobility, when compared with GaAs and other materials, results in low sensitivity. Oxide defects result in flicker or 1/f noise, complicating the detection of DC or low-frequency signals. Finally, CMOS magnetic sensors have offsets (in voltage or current), resulting from the fabrication process. These effects result in a smaller signal and more noise, when compared with other sensor technologies.

There are additional challenges that come from the measurement system. The detection of paramagnetic beads requires a polarization field. This field is two to three orders of magnitude larger than the signal generated by the bead, and parasitic coupling in the measurement system results in a output signal even when no bead is present. Even with careful design to minimize parasitic coupling and the use of differential circuitry, this leakage signal is many times larger than the signal from the magnetic bead.

2.2 Magnetic-Bead Signal

2.2.1 Magnetic-Field Calculation

The signal produced by a magnetic bead resembles a magnetic dipole. However, the beads produce a field only when induced by an external polarization field, and

therefore are paramagnetic. If the field of the bead is modeled as a magnetic dipole, the magnitude of the magnetic field, aligned with the polarization-field vector, is:

$$B = \frac{2M}{cz^3}$$

Here, B is the magnetic field, z is the distance for the center of the bead, c is the speed of light, and M is the magnetization. The field decays in proportion to the cube of the distance z, so the beads should be as close as possible to the sensor. The magnetization M is determined by the bead properties and the polarization field H:

$$M = \chi H v$$

Here, χ is the susceptibility and v is the volume of the bead. The susceptibility is proportional to the magnetite concentration of the bead, and ranges from approximately 0.2 to 5 for commercially available beads. Measured magnetization for various beads has been published (Baselt et al., 1998). The magnetization is linearly proportional to the polarization field for small fields, but ultimately saturates. The level at which the induced field saturates, commonly called the saturation magnetization, is a function of a number of parameters, including the magnetite concentration of the bead, and the bead construction (e.g., solid or powder core). This saturation typically occurs for polarization fields less than 100 kA/m, and is proportional to the magnetite concentration.

2.2.2 Magnetic-Field Simulation

The dipole model is only valid for far-field calculation, where the bead radius is not significant. For more accurate estimates of the bead field, a magnetic simulator can be employed (*MagNet*, Infolytica, Montreal, Canada). Figure 2.1 shows the simulated

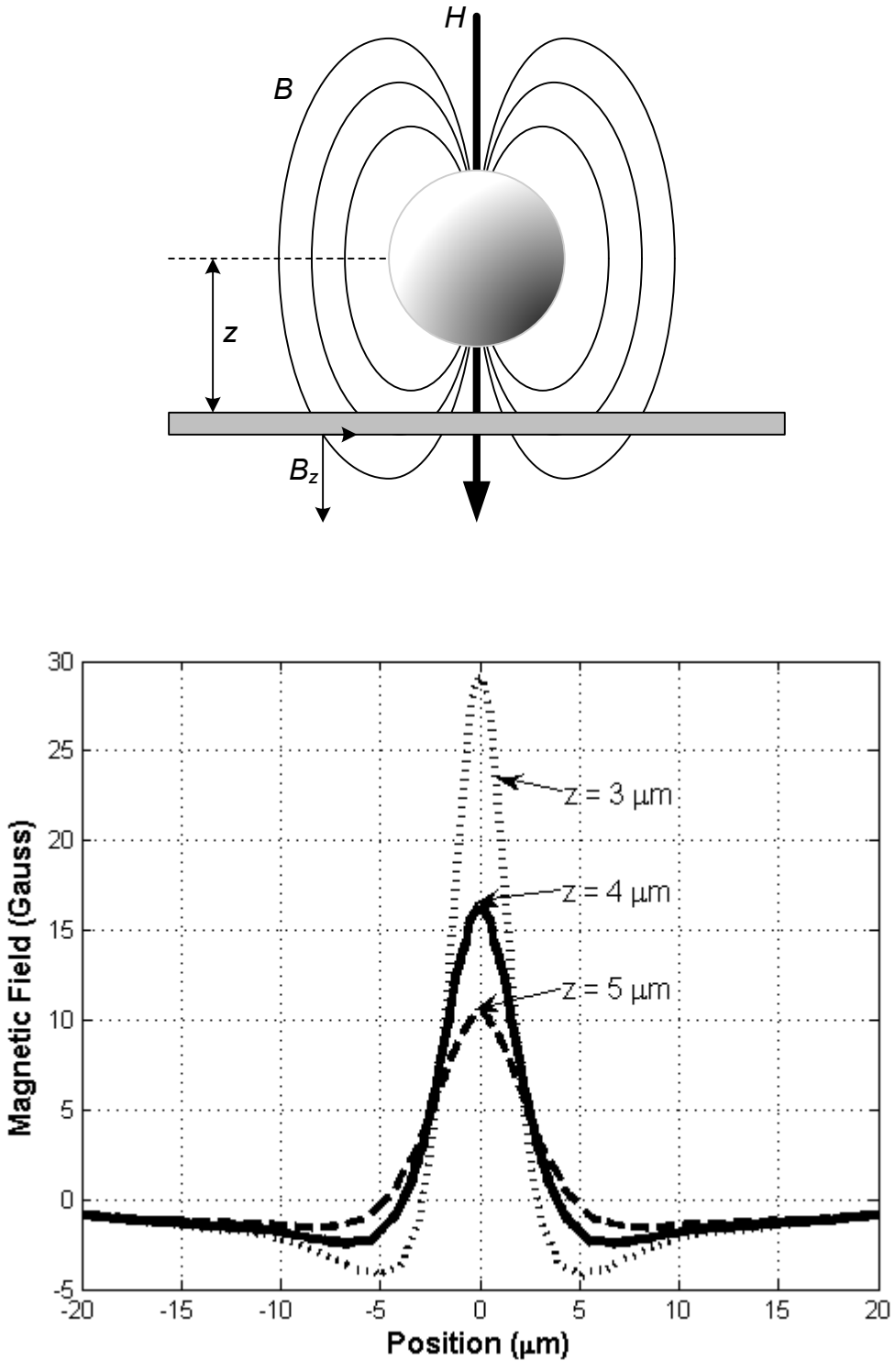

Figure 2.1: Simulated magnetic field vs. position for a 3-μm, 15% magnetite bead (χ = 0.75) placed 3, 4, and 5 μm above a plane, with a 35-kA/m polarization field.

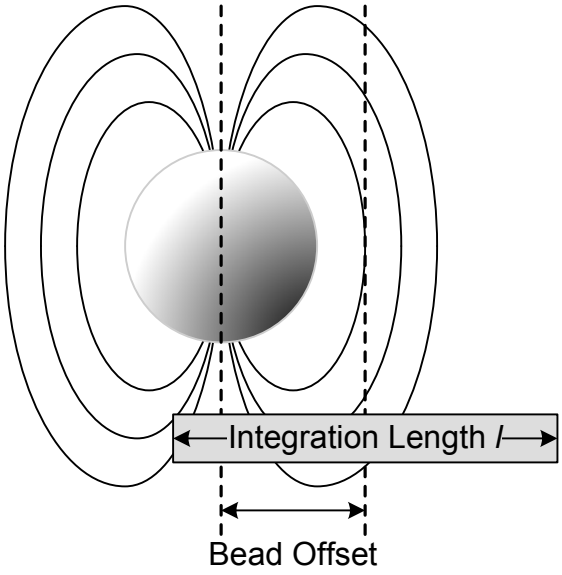

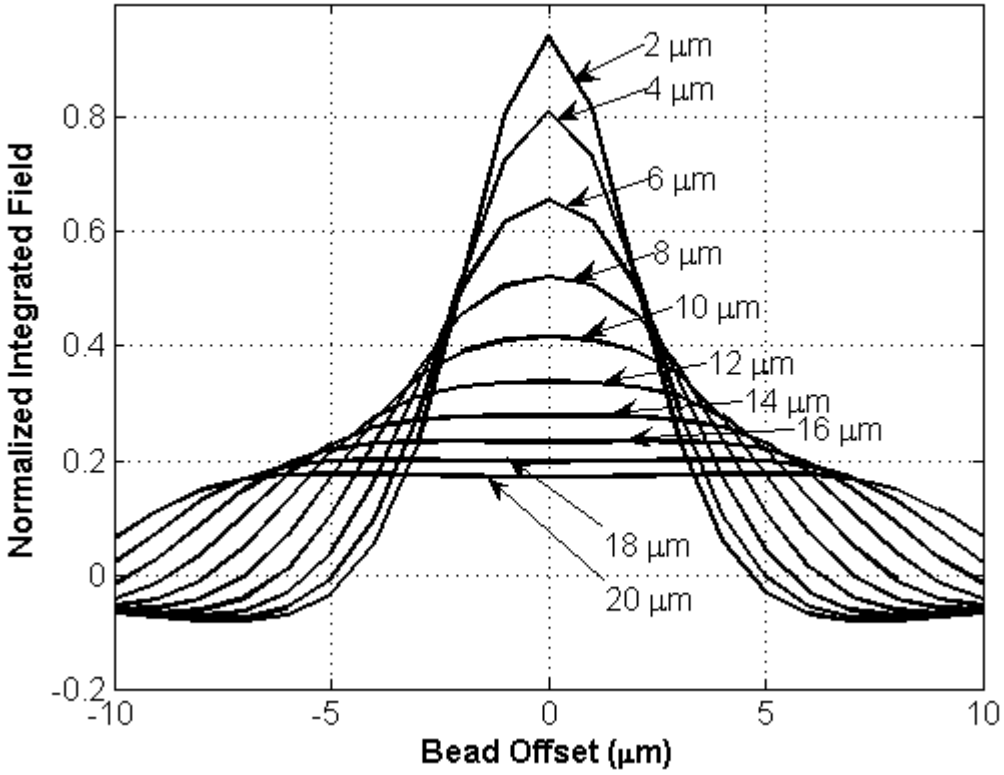

Figure 2.2: Selected line integrals of lengths (*l*) from 2 μm to 20 μm, vs. bead position offset, for bead parameters as in Figure 2.1 (z = 4 μm).

response to a 35-kA/m polarization field for 3-μm diameter, 15% magnetite bead (χ = 0.75) placed 3, 4, and 5 μm from a plane. The strong dependence on z is evident. For z = 4 μm, the peak field is approximately 5% of the polarization field. In this system, the polarization field is normal to the measurement plane. When the bead is above the measurement plane, the resulting field in the plane is trimodal with one positive and two negative peaks. This field integrates to zero when taken over an infinite plane.

From Figure 2.1, two effects are important to consider for successful detection of the bead. First, a magnetic sensor integrates the field over the sensor area, so device dimensions must be matched to the field from the bead. Second, the bead may be offset from the center of the sensor, significantly changing the field in the sensor area. Figure 2.2 shows the line integral over selected integration lengths l from 2 μm to 20 μm, as a function of the bead offset from the center of the integration limits. The line integral is linearly proportional to the Hall voltage, though effects of non-uniform current density in the device are not considered. The results were normalized by the peak field from Figure 2.1 (z = 4 μm) in order to show reductions in the signal that come from the integration of a non-uniform field. As expected from the narrow width of the signal peak in Figure 2.1, longer line integrals (i.e. larger Hall devices) loose signal, but are less sensitive to bead offset. However, in an array of sensors, a bead offset from one sensor will likely be detected by a neighboring sensor.

2.2.3 Dynamic Effects

The noise performance of many magnetic sensors improves with operating frequency. This suggests that a higher polarization-field frequency will improve

detection. However, as will be shown in Section 3.3.2, magnetic beads show some reduction in signal at higher polarization-field frequencies. Recently, dynamic effects on magnetization *M* have been modeled using complex susceptibility (Fannin et al., 2005):

$$M = \chi(\omega)Hv$$

Once polarized, a magnetic bead has energy associated with the dipole alignment that is linearly proportional to the bead volume *v*. De-alignment of the dipoles occurs through thermal fluctuations, resulting in the Neel relaxation time constant of:

$$\tau = \tau_0 exp\left(\frac{Kv}{kT}\right)$$

Here, *K* is the anisotropy constant of the particle. Smaller particles have less energy associated with dipole alignment, and therefore relax more quickly. In the system used in this work, two significant distinctions exist when compared with the relaxation-time measurements presented in Fannin et al. First, beads are immobilized on the sensor surface during measurement, so their motion is constrained significantly. Second, the polarization field is sinusoidal and continuous. The relationship between relaxation time in the absence of a polarizing field and the frequency response to a dynamic polarizing field has not been studied. Therefore, more investigation is needed to better understand this effect.

2.3 CMOS Magnetic-Sensor Design

2.3.1 Topology Selection

The CMOS fabrication technology used in the sensor chip supports standard NMOS and PMOS transistors, as well as polysilicon, N-type, and P-type resistors. No

specialized magnetoresistive devices are available, so the Hall-Effect is the only available mechanism for magnetic field sensing. In the CMOS process used, this type of sensor can be implemented with either a diffusion layer (e.g. N-Well) or a MOS transistor. The lightly-doped N-Well implant results in higher carrier mobility and lower 1/f noise. However, it is difficult to integrate into an array of sensors, where row and column decoding mechanisms are required. Instead, an NMOS transistor implementation was chosen (Popovic, 1991). This allows the gate to be used to enable an element in the array. The sensor design chosen resembles a standard NMOS transistor, except with four contact regions. Current flow can occur between either opposing pair of contacts. The presence of a magnetic field deflects this current, and a Hall voltage is measurable across the other opposing pair of contacts. A general expression for the output signal of this device is:

$$V_O = \mu_H \mathrm{G} V_B B_\perp$$

Here, μ_H is the Hall mobility, G is a geometric factor that accounts for non-uniform current density, V_B is the bias voltage, and B is the field normal to the sensor plane. For a device of equal length and width, G is approximately 0.7. The field response shown in Figure 2.1 shows the positive and negative peaks spaced by approximately 6-μm. In order to measure this field profile, but reject signals generated by the polarization field, a two-sensor structure is employed (Figure 2.3). The arrows show that the relative current flow between two sensors remains orthogonal, so that the magnetic field common to each sensor is largely cancelled. However, magnetic field differences between the two sensors are measured.

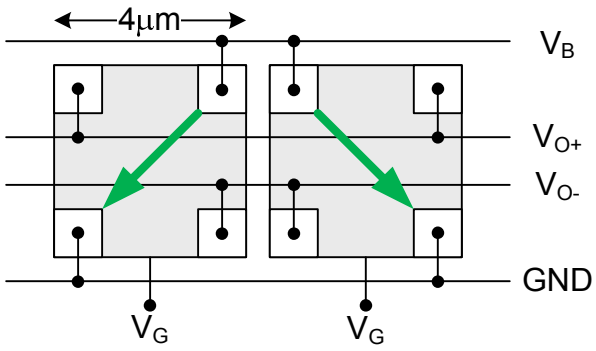

Figure 2.3: Differential Hall-Sensor structure, with orthogonal current flow (arrows), contact area (white), and gate area (gray).

Each Hall sensor has five terminals; gate voltage input, drain bias input, ground, and a differential voltage output. The gate voltage is used in the implementation of the sensor array column decoding. When gate terminal is grounded, the sensor device is off and a high resistance exists between the four other terminals. When the gate voltage is connected to the positive supply, the sensor device is in on. The maximum drain bias is set so that the sensor operates as a resistor.

2.3.2 Sensor Design Parameters

Figure 2.4 shows line integral pairs (parameters as in Figure 2.1, z = 4 μm) as a function of bead offset, for selected lengths from 2 μm to 8 μm. The difference in the two integrals is plotted, corresponding to a differential sensor. The differential output is zero when a bead is centered between the two sensors, since each individual sensor produces a signal that is equal and opposite of the other. The 2-μm sensor produces the largest signal when configured as a single sensor, but looses signal as a differential structure. The 4-μm

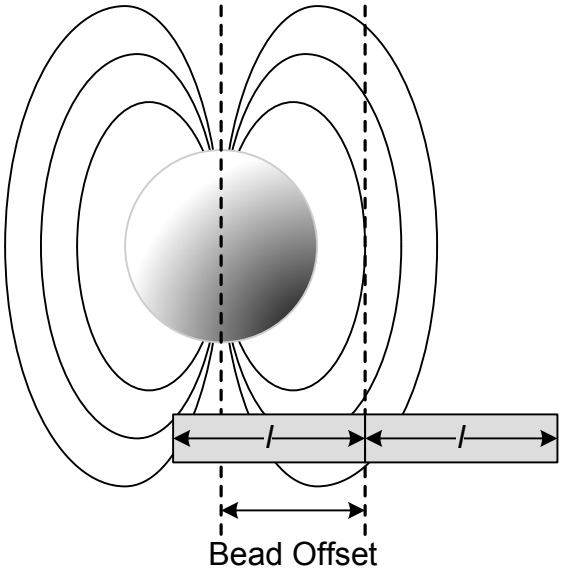

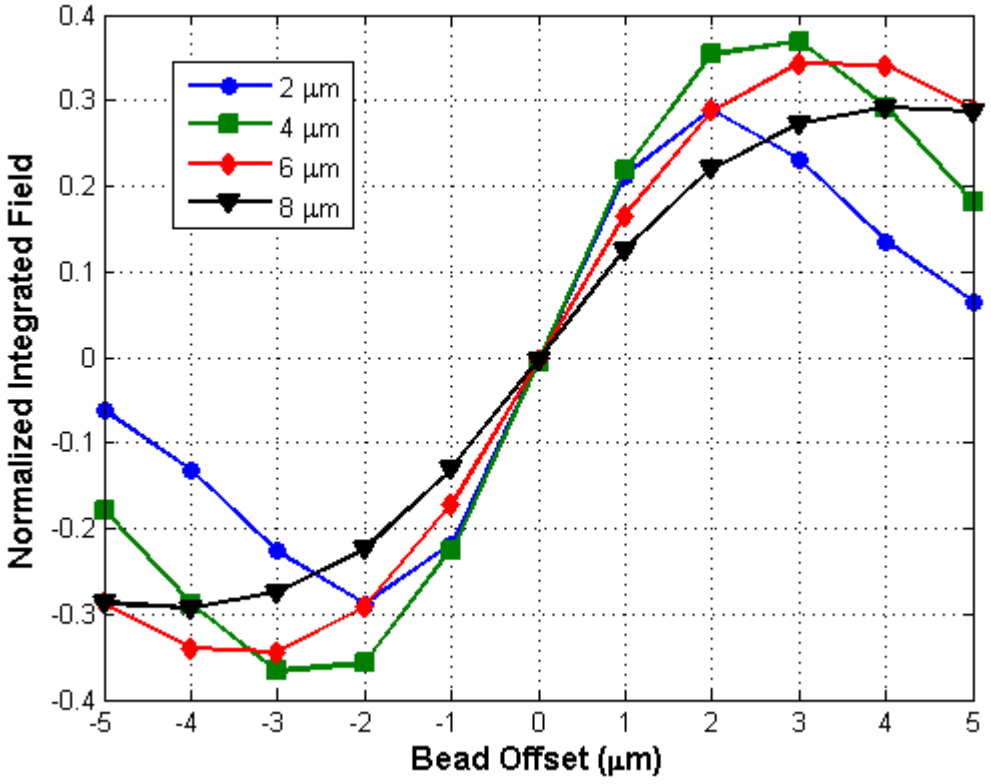

Figure 2.4: Selected line integral pairs vs. bead offset, for integration lengths (*l*) of 2 µm - 8 µm. The difference in the two line integrals is shown, corresponding to a differential sensor. Bead parameters as in Figure 2.1 (z = 4 µm).

dimensions were chosen to match the response of field induced by 3-μm beads. With these dimensions and optimal bead placement, the signal from the parameters in Figure 2.1 (z = 4 μm) is estimated at 35% of the uniform field, corresponding 6 Gauss. This reduction in signal occurs due to the non-uniform field from the bead and the differential sensor implementation. Placing sensors next to each other improves device matching and consequently rejection of the polarizing field. However, the output of one Hall sensor is loaded by the output impedance of the other, reducing the signal by 50%. Alternatively, a pseudo-differential structure could be employed to increase the signal at the expense of matching performance.

The DC sensitivity of the sensor was measured to be 2.6 mV/kGauss with a drain bias of 0.4V, a gate bias of 2.5V, and a drain current of 70 μA per sensor (140 μA for the differential structure). The measured sensitivity is consistent with prediction. The value corresponds to a uniform field applied to the entire sensor area, which is equivalent to a zeroth-order approximation of a magnetic bead signal.

2.3.3 Sensor Noise

Noise is the CMOS sensor comes from thermal and 1/f sources. In simulation, a simple model was used to estimate the noise contribution from the sensor. Two 4-μm/2-μm NMOS devices were placed in series, each with gate bias of 2.5 V, and drain bias of the top device of 0.4 V. The noise voltage was taken from the intermediate node. Next, the amplification circuitry following the sensor was sized to contribute approximately 30% of the output noise at 2-kHz, corresponding to 32 nV/$\sqrt{Hz}$. In measurement, the

amplification circuitry was found to be 60% of the output noise, or 45 nV/$\sqrt{Hz}$. The noise of the sensor at 2-kHz was predicted to be 45 nV/$\sqrt{Hz}$, compared with the measured value of 26 nV/$\sqrt{Hz}$. The measurement corresponds to a magnetic detection noise floor of 0.1 Gauss/$\sqrt{Hz}$ (10 μT/$\sqrt{Hz}$). These results suggest that our 1/f noise simulation models significantly overstate the actual noise. One possible explanation of this is the device symmetry of the diamond-shaped sensor. The four-terminal configuration of the sensor may result in different 1/f noise properties than the simple three-terminal model. Oxide traps along the centerline of the diamond-shaped sensor appear as common mode noise to the voltage outputs. Noise at each output terminal is partially correlated to that at the other terminal, resulting in a reduction in differential noise. However, direct comparison of a three-terminal and four-terminal device is required before drawing conclusions.

2.4 System Design

2.4.1 Sensor-Chip Architecture

To enable a quantitative measurement system, and to provide a larger area for bead binding and detection, an array of sensor elements was implemented. By counting the number of array elements that receive a signal from a bead, the number of beads in the measurement area can be approximated. Figure 2.5 shows schematic diagram of the biosensor chip architecture. It consists of a 32 x 32 array of magnetic sensors and peripheral circuitry. The sensor array pitch is 10 μm in the X direction and 5.5 μm in the Y direction, resulting in a total active area of 0.07 mm^2.

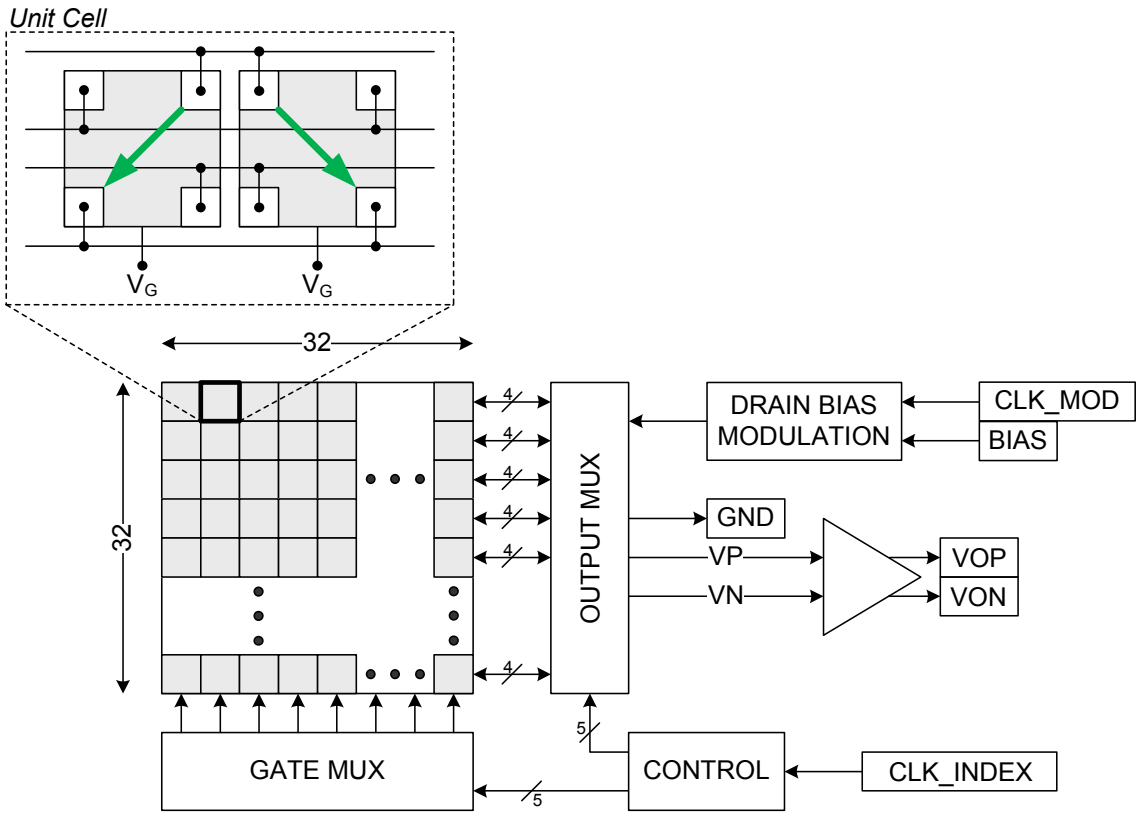

Figure 2.5: Schematic of sensor chip architecture with 32 x 32 array, and expanded detail of an array cell.

The array is scanned by control of the gate (column) and output (row) MUXs. The drain bias controls the current flow in the sensor, and allows row selection. The output MUX is implemented by per-row NFETs with shared drain connections, where decoding circuitry controls the gate voltage of these devices. The array index increments at approximately 8 Hz. Consequently, a complete scan of all 1024 elements takes approximately two minutes. Fewer elements can be scanned to reduce the measurement time. The differential output signals are amplified by approximately 30 dB before being sent off chip.

The sensor elements in the first column of the array are connected so that the two sensor signals add together, resulting in the measurement (rather than cancellation) of the polarization field. The measurement of the polarization signal provides a calibration reference for the software algorithm.

2.4.2 Electrical Modulation

The presence of a large polarization field results in parasitic coupling (leakage) to almost every part of the measurement system. Even without a sensor-chip module inserted in the test socket, the 2.03-kHz polarization signal can be detected by the interface circuitry. Though this signal could be calibrated, it is dependent on the position of the electromagnet in reference to cables and other variables in the experimental setup. To reduce the effect of the signal, the drain bias of the sensor is modulated at 16 kHz. This modulation results in the upconversion of the 2.03-kHz signal to 16 kHz +/- 2.03 kHz. The parasitic coupling from the polarization signal remains at 2.03 kHz, so it no longer affects the measurement. The modulation uses a square wave that switches the drain voltage between 0 V and 0.8 V.

In addition to mitigating the effects of leakage from the polarization signal, drain modulation also provides a modest improvement in noise performance. For the same average drain current, the overall system SNR is improved by approximately 6 dB. This comes from two mechanisms. First, the 1/f noise contribution of the PMOS amplifiers is reduced by the upconversion, since the amplifier noise at 16 kHz is lower than at 2 kHz. Second, the drain modulation provides approximately 3 dB improvement in SNR of the sensor alone. The 1/f noise dependence on gate bias has been described in literature and

is included in many transistor noise models, such as BSIM3 (Erturk et al, 2006). However, a drain bias dependence (other than through changes in drain current) has not been described.

2.5 Sensor-Chip Fabrication

2.5.1 CMOS Processing

Fabrication of the biosensor chip starts with complete processing in a single-poly non-epi CMOS foundry with five aluminum metal layers and 0.25-μm lithography. In order to improve the performance of the biosensor, additional processing steps are performed after the standard CMOS fabrication. First, the distance from the chip surface to the sensor is reduced to 2.5 μm by thinning the dielectric above the sensor. This increases the signal from the magnetic beads. Second, a gold layer is used on the chip surface to improve protein adsorption (Anwar et al., 2005). The design objective was to limit post-processing steps in order to preserve the economic advantage of CMOS technology. These steps were relatively limited in scope when compared with the standard processing required for CMOS fabrication. No small-feature lithography was required, and no CMOS-incompatible films were deposited. Non-standard use of the passivation mask allows for simplified post-processing. Figure 2.6 shows details the mask definition and resulting chip cross section. Normally, the passivation opening is only drawn over a bonding pad, which serves as an etch stop for the Reactive Ion Etch (RIE). In this design, an additional opening is drawn over the sensor area, which results in over-etching the SiO_2 Inter-Layer Dielectric (ILD) above the sensor area.

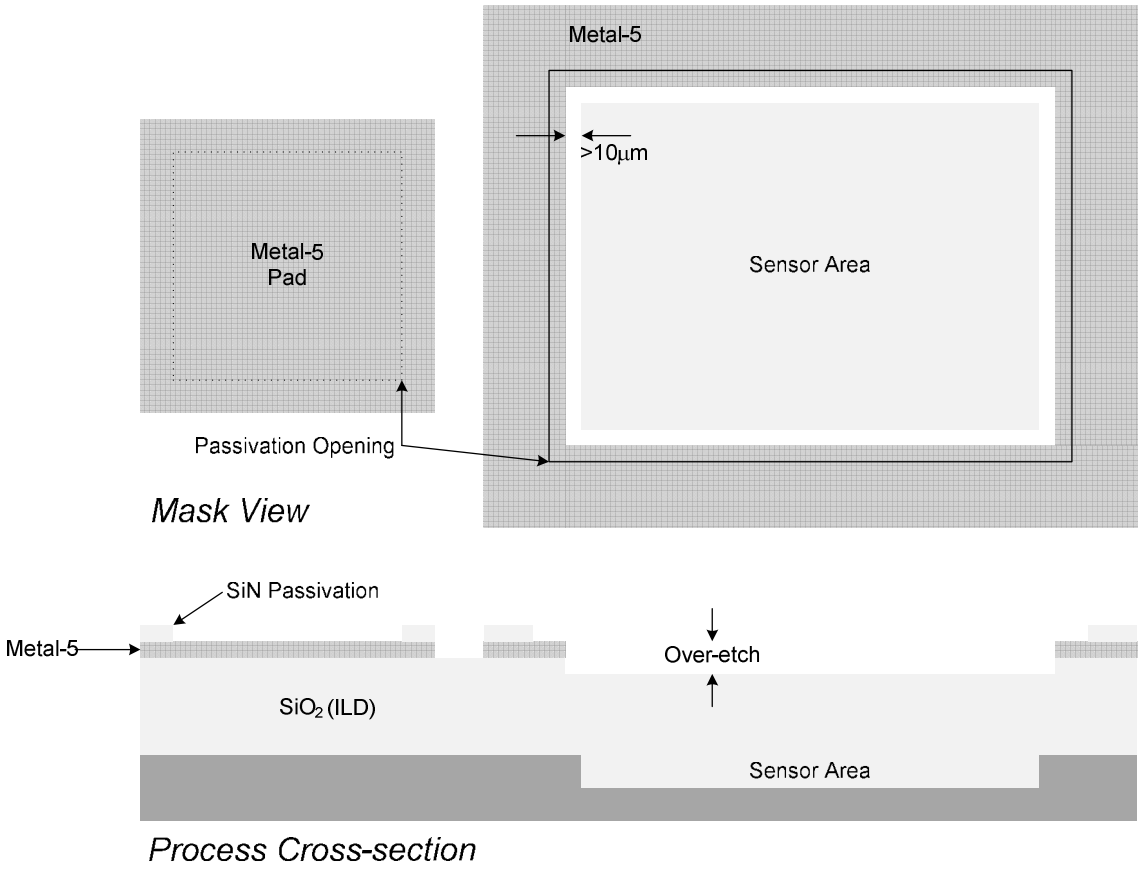

Figure 2.6: Non-standard use of passivation mask in standard CMOS processing results in over-etching into the oxide over the sensor area.

2.5.2 Post-Processing

Additional processing was performed on wafer fragments that contain 6 biosensor chips, measuring 5 mm x 7.5 mm. Each chip measures 2.5 mm x 2.5 mm. The wafer fragments were mounted on a carrier wafer for some processing steps. Figure 2.7 shows additional detail of the post-processing steps as outlined below, and in Appendix A:

(A) Photoresist was applied by hand using a resist pen, in order to protect the bond pads during subsequent etch steps (Figure 2.7A). Metal-5 served as a hard mask

that defined the sensor area, but was drawn at least 10 μm outside of the sensor array. This gap prevents beads trapped in the corners of the etched surface from being detected by the sensor. The inter-layer dielectric (ILD) above the sensor was reduced by RIE with Metal-2 serving as an etch-stop (Figure 2.7B). The anisotropic plasma etch resulted in nearly vertical sidewall definition, so that the sensor area remained mostly defined by the Metal-5 pattern.

(B) The plasma etch was followed by a short (~2 min) liquid aluminum etch, with the TiN seed layer serving as an etch stop (Figure 2.7C). Though this seed layer is thin (<100 nm), this is a highly selective etch. This step accomplished two functions: first, it further reduced the distance to the sensor. Second, it provided a smoother surface than aluminum for subsequent processing steps.

(C) A 50-nm layer of gold was applied using evaporation deposition. A 7-nm chrome seed layer was used for adhesion, and a coarse, re-usable hard mask was employed to define that pattern (Figure 2.7D). The gold layer improves bio-compatibility and protein adsorption (Figure 2.7E). Gold bumps were applied to the bond pads using a wire bonder (Figure 2.7F). The addition of gold bumps to the aluminum pads provided compatibility with standard solder types, such as Sn63Pb37, that are used in flip-chip assembly.

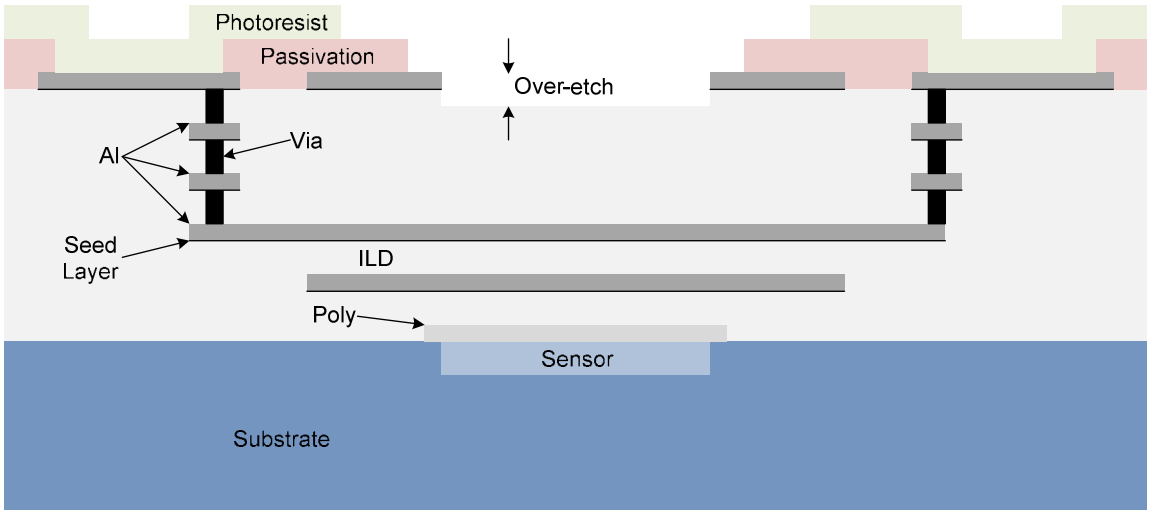

Figure 2.7A: Photoresist applied by resist pen protected passivation around aluminum bond pads.

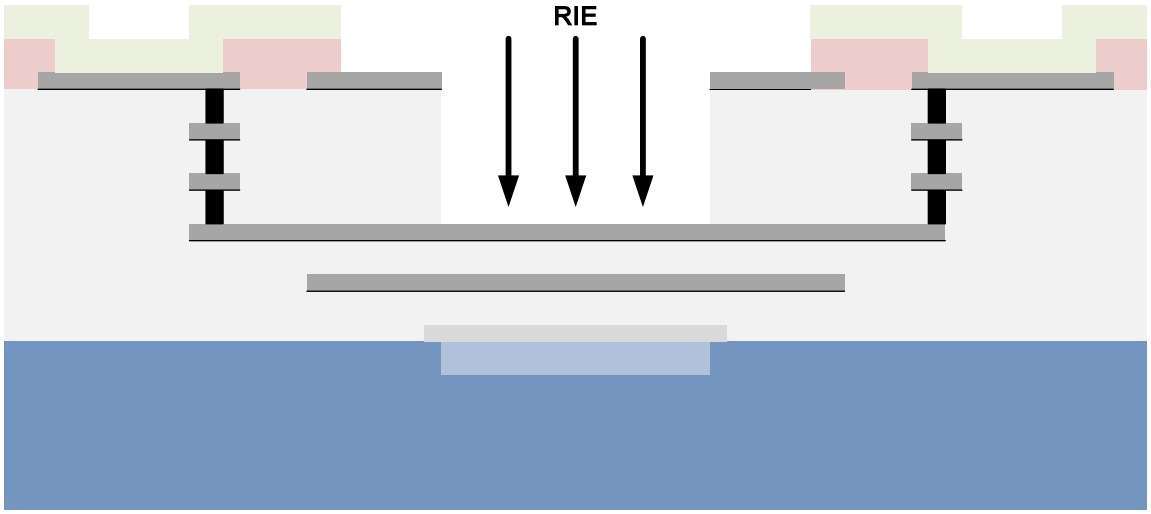

Figure 2.7B: Reactive Ion Etch (RIE) with Metal-5 hard mask and Metal-2 etch stop.

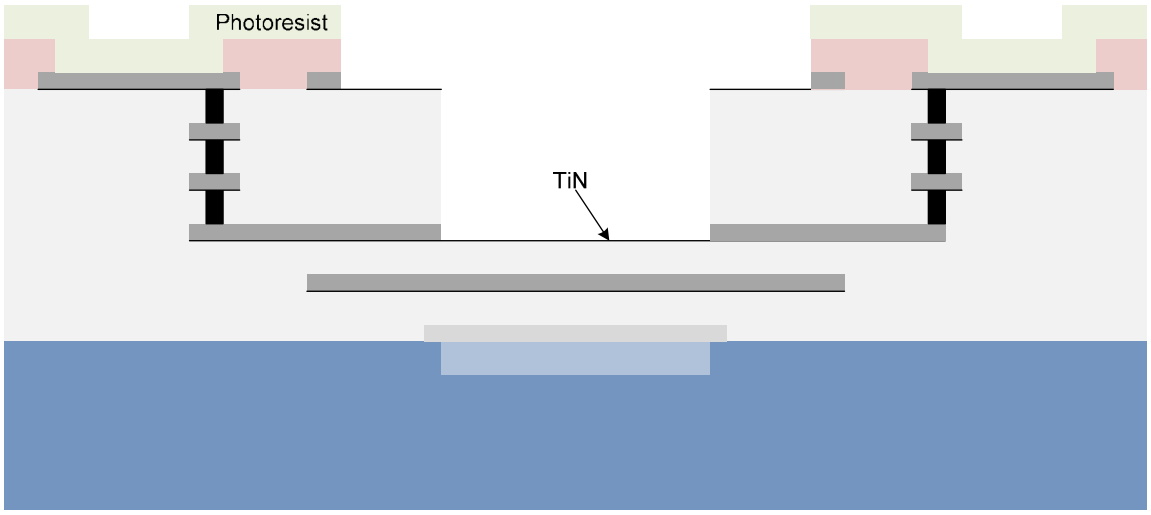

Figure 2.7C: Aluminum wet-etch removed Metal-2 over the sensor area, but was selective against the TiN seed layer.

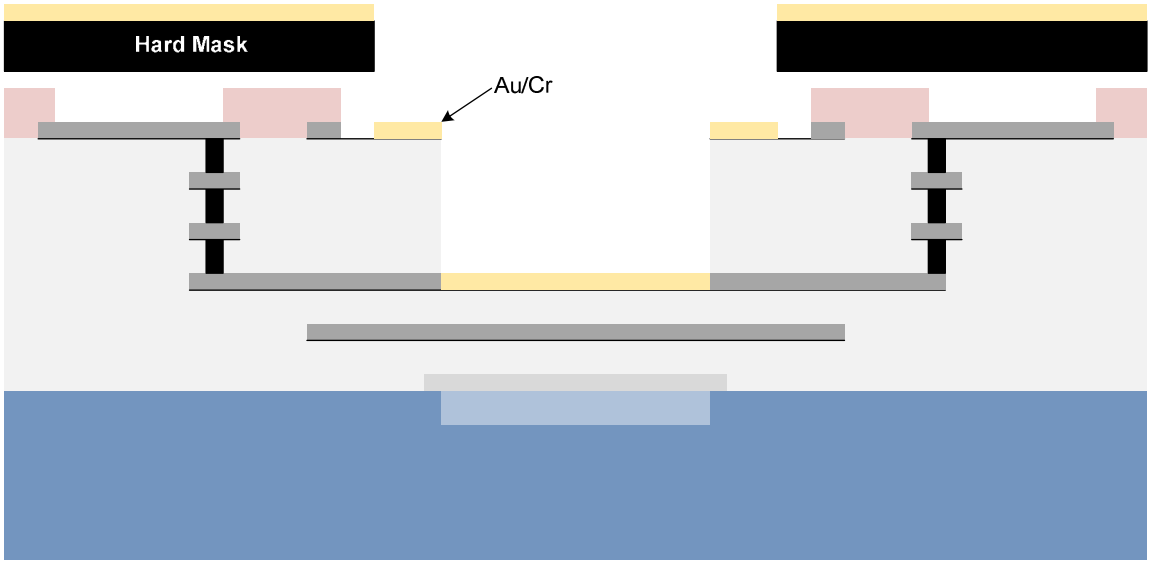

Figure 2.7D: Reusable hard mask was employed during evaporation deposition of Au/Cr layers.

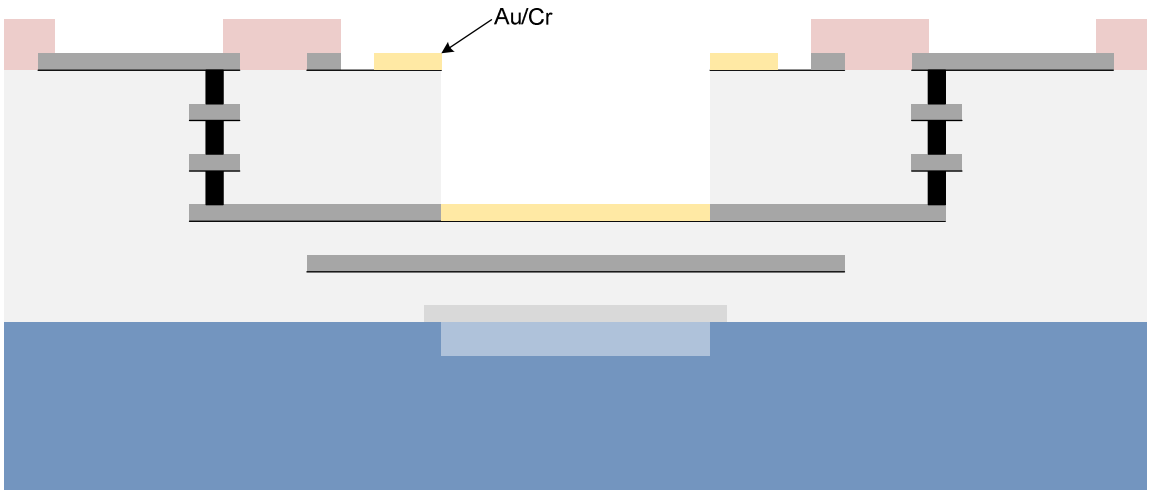

Figure 2.7E: Final structure after post processing.

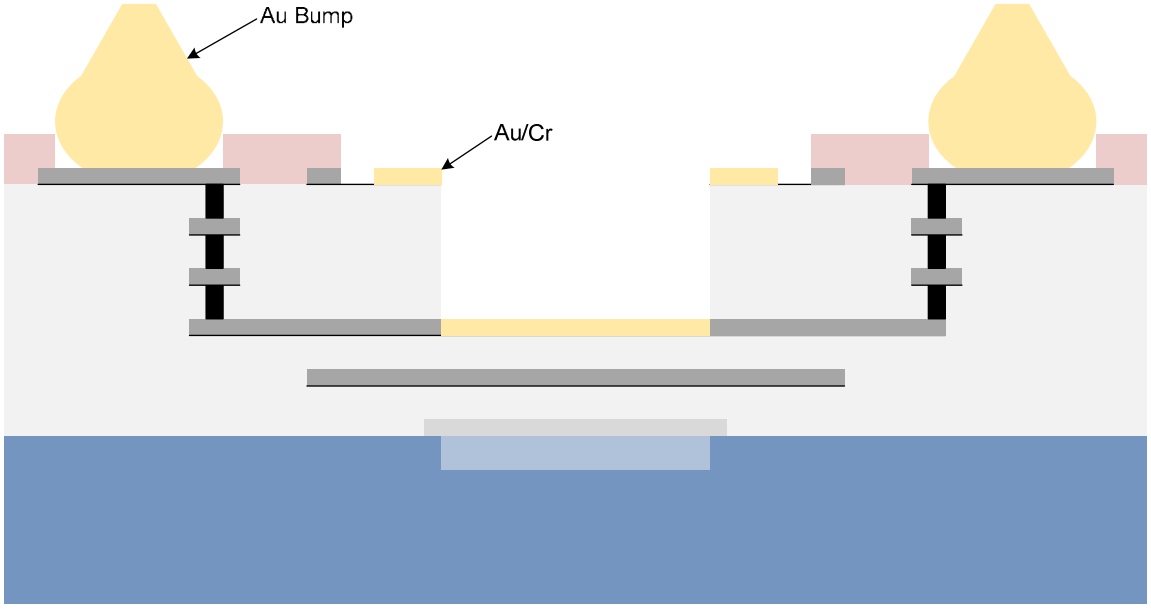

Figure 2.7F: Addition of gold bumps to enable assembly with PCB.

2.6 Fluidic Packaging and Module Assembly

In order to make the sensor chip compatible with the fluidic samples, a module was designed. The sensor module design also followed the philosophy of utilizing existing technology in the electronics industry. The sensor module, including integrated

sample well, is based on standard Printed Circuit Board (PCB) fabrication. A side and bottom view drawing of this is shown in Figure 2.8. The dimensions of the sensor module are 2.5 x 1.5 x 0.65 cm. The assembled module is intended for single use. Though reuse is possible, avoiding sample contamination from the previous use requires a complicated cleaning process. The fluid sample is contained the integrated 150-µl fluid-sample well, and contact with the sensor surface is made through a 2-mm hole at the bottom of the well. A significantly smaller fluid-sample well could be employed, as dictated by a particular assay. The sensor chip is flip-chip mounted to the gold contact pads on the PCB module, enabling the necessary electrical signals to be routed to the edge-card contacts. The gold bumping and flip-chip assembly was accomplished through an outside service company (Corwil Technology Co., Fremont, CA), using standard flip-chip assembly equipment. The epoxy underfill isolates these electrical contacts from the fluid sample. This process was done by hand, due to the risk of obscuring the sensor area with epoxy. However, precision dispensing equipment should be configurable to achieve reliable results.

Expanded detail of the sensor chip to PCB interface is shown in Figure 2.9. Solder was applied to the gold contact pads of the PCB using a stencil. The sensor chip was aligned with the PCB using flip-chip assembly equipment. Next, solder was reflowed according the manufacturers specifications. After flip-chip assembly by the outside service company, underfill epoxy (*Duralco 4525*, Cotronics Co., Brooklyn, NY) was applied by hand. The use of underfill epoxy after flip-chip assembly served two functions: First, it provided necessary mechanical strength. Second, it provided isolation between the fluid and the electrical signals. The epoxy was initially cured at 125 °C while

the viscosity was monitored to achieve electrical isolation without obscuring the sensor area, typically 3-5 minutes. Next, the same epoxy was used to coat the sample well in order to limit analyte exposure to low-quality gold plating on the PCB sidewall. After this, the epoxy was cured at 60 °C for 4 hours.

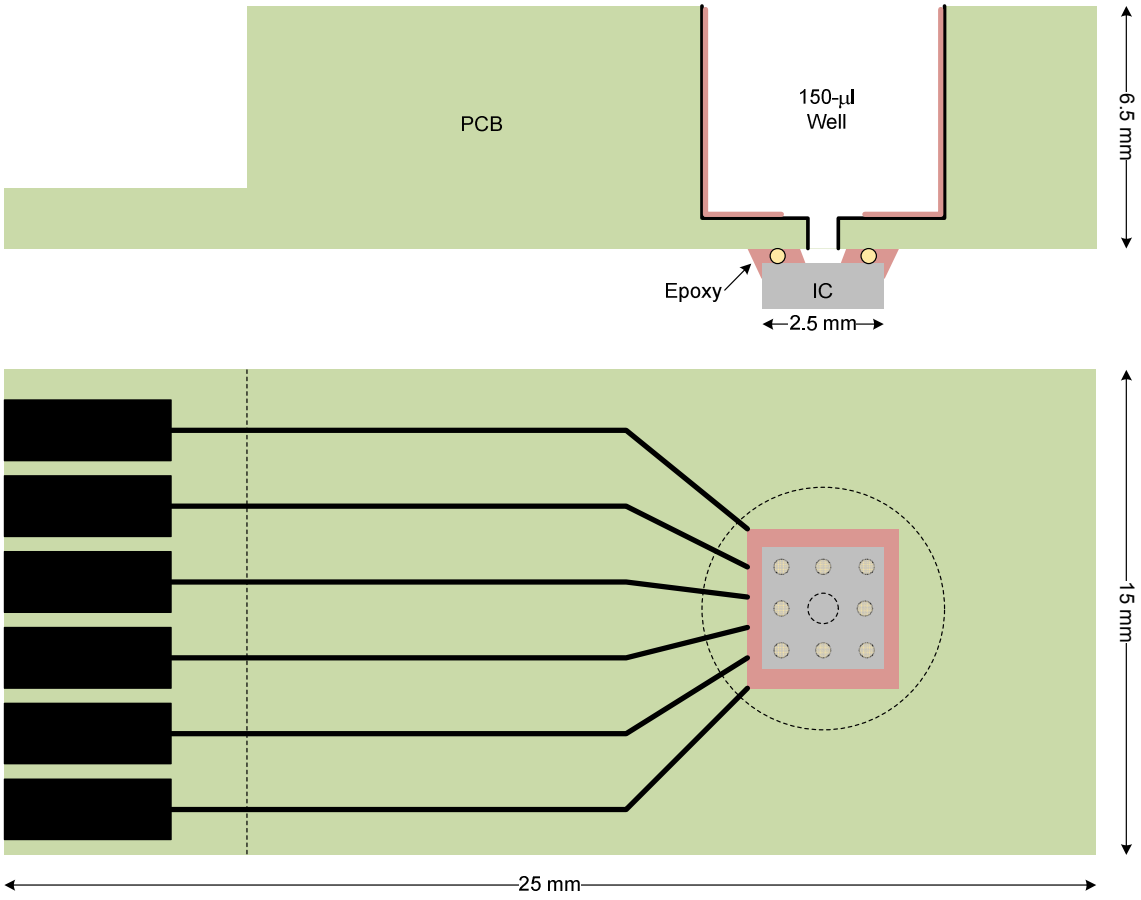

Figure 2.8: Sensor module cross-section (top), and bottom-view (bottom), consisting of sensor chip (gray), PCB (green) with metal routing and pads (black), and assembly epoxy (red).

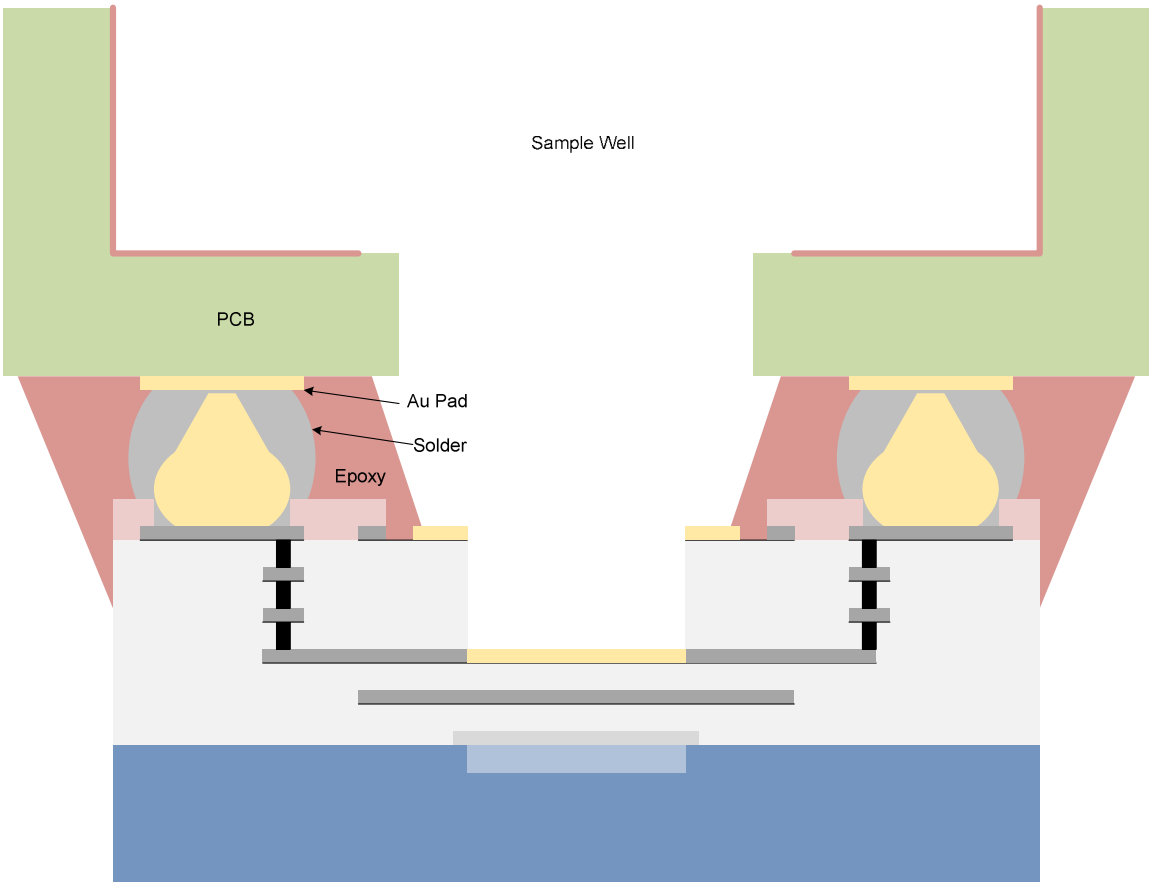

Figure 2.9: Expanded detail of sensor-chip-to-PCB interface, including flip-chip assembly employing gold bumps, standard Sn63Pb37 solder, and epoxy isolation.

2.7 Measurement System

2.7.1 Reader Hardware

The disposable sensor module is measured by a reader system. A schematic of the entire platform is shown in Figure 2.10. It consists of a custom-made electromagnet, an audio-range power-amplifier (Parasound, San Francisco, CA), a DC power supply (Hewlett Packard, Santa Clara, CA), interface electronics, an audio codec with USB interface (M-Audio, Irwindale, CA), and a laptop computer. The interface electronics

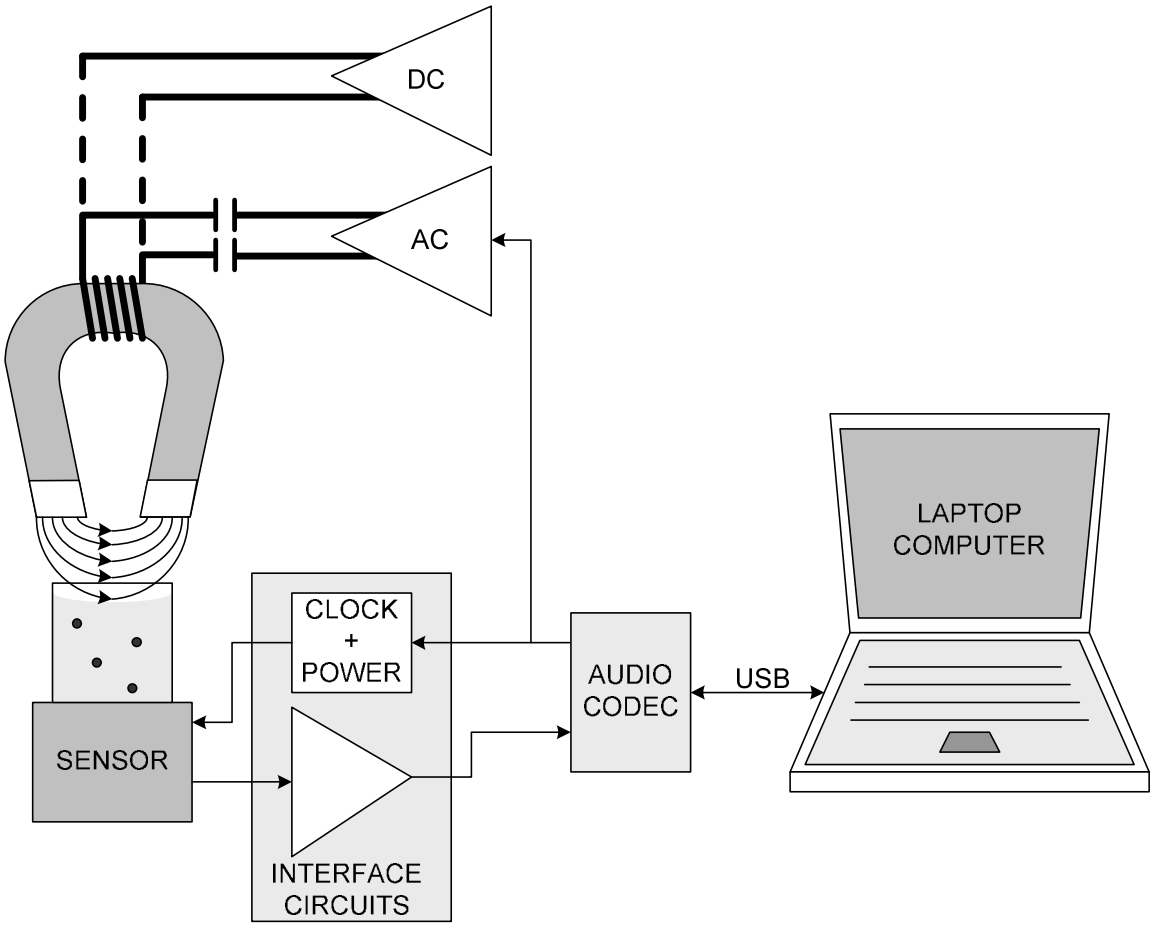

Figure 2.10: Measurement system, consisting of a laptop computer, audio codec, interface electronics, and electromagnet driven by an AC amplifier (detection) or DC current source (magnetic washing).

consists of reset circuitry, clock generation, and amplification. The laptop computer generates and processes digital signals according to customized software code running in Matlab™ software (The Mathworks, Warwick, RI). The audio codec provides high-quality conversion from analog-to-digital and digital-to-analog domains, and uses a standard USB interface. Though many laptop computers come with integrated audio codecs, the quality and function varies significantly between different manufacturers.

During measurements, the laptop computer produces a 2.03-kHz sinusoidal output in a digital format that is converted to an analog output by the audio codec. This signal is amplified by the power amplifier, which drives the electromagnet through a capacitor, forming series-resonant network. This network transforms the 26-mH inductance of the electromagnetic to a resistance of approximately 4 Ohms at 2 kHz. The electromagnet generates a polarization field of approximately 35-kA/m field across a 1-cm gap. The signal from the sensor module is AC-coupled and amplified by approximately 16 dB before being sent to the audio codec. The audio sampling rate is set to 44.1 kS/sec with a resolution of 16 bits. Much of the dynamic range requirement comes from the residual carrier leakage from the upconversion process. With device mismatch of a few percent and 0.8-V modulation, this signal is typically in the range of 10 mV at the sensor output. This value is approximately 50-60 dB larger than the signal from the bead.

2.7.2 Magnetic Washing

In addition to the polarization field used during measurement, a DC field and gradient is required to produce appropriate force for magnetic washing. The force on a magnetic bead can be expressed as:

$$F = MH\left(dB/_{dz}\right)$$

Here, *dB/dz* is the field gradient normal to the sensor plane. During measurement, the electromagnet design results in a weak gradient upward. This implementation was found to prevent non-specifically bound beads from becoming strongly attached to the surface during measurement. During the magnetic washing steps of the protocol, a DC current source is used in place of the audio amplifier. A small attachment is added to the

electromagnet to produce a high-gradient field that increases the pulling force on the beads (Figure 2.11). This attachment is not desirable for measurement, since a nearly uniform field is required to avoid disturbing the bead positions. The additional flux-concentrator bars pull the field lines away from the centerline, resulting in the high gradient. The resulting system produces field gradients of approximately 500 Gauss/cm at a bias current of 2.5 A. The optimal force depends on assay parameters, as described in Chapter 3. The force is adjusted by changing the bias current.

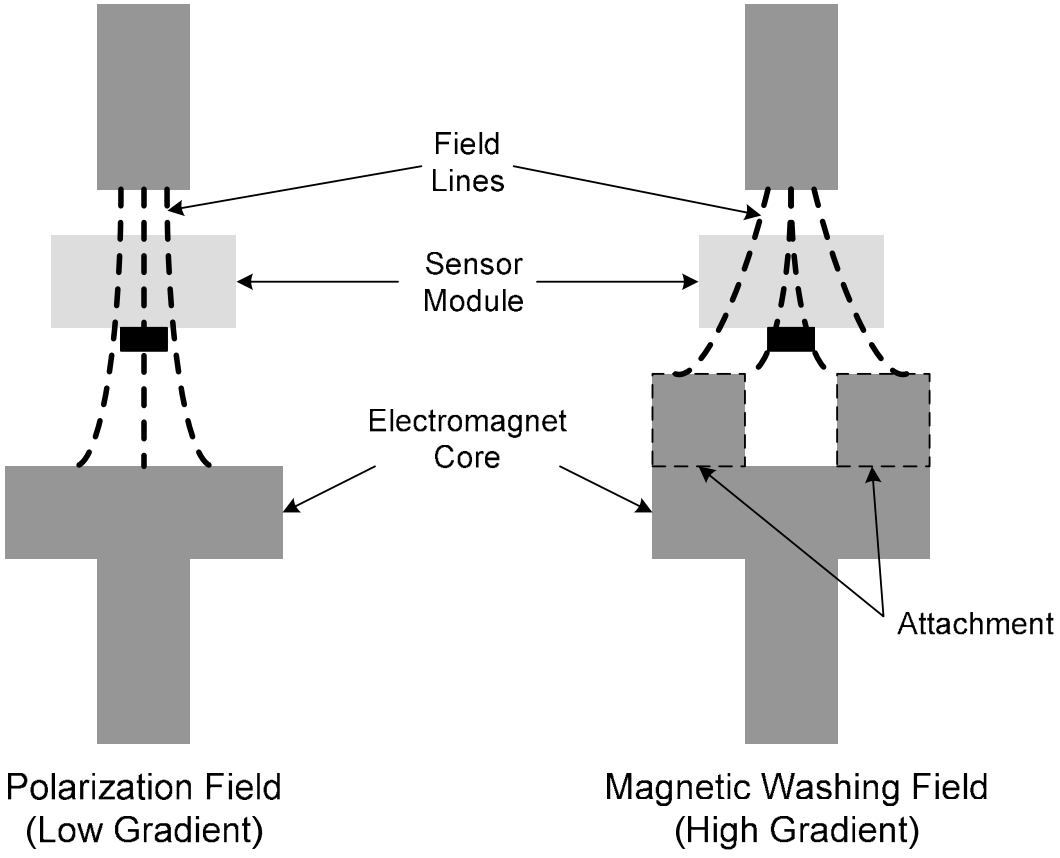

Figure 2.11: Electromagnet configuration for bead polarization (left) and magnetic washing (right).

2.8 Software and Calibration Algorithms

2.8.1 Error Sources and Calibration

The intrinsically low sensitivity of the CMOS Hall-Effect sensor can be improved through measurement technique. The 2.03-kHz sinusoidal polarization signal allows the measurement to use a small bandwidth around the signal frequency to improve the signal-to-noise ratio (SNR). However, there are some limitations of the measurement system that need to be compensated for in software. First, the polarization signal is not perfectly cancelled by the two-sensor structure, so that a residual signal exists in the output even if no bead is present. Without correction, this signal is typically much larger than the signal from a bead. The mismatch between the two sensor elements is random, so that each array element has a different leakage level. To correct for this, the sensor module is first measured without beads to establish a baseline response. This measurement is stored in the software.

The second limitation of the measurement system is that the polarization signal is time varying. This is due to changes in temperature of the electromagnet core during operation. The field of the electromagnet is strongly dependent on core temperature, so this effect can result in greater than 10% change in field strength during operation. However, the temperature change occurs relatively slowly (~minute) due to the large thermal mass of the core. In addition to this effect, the current protocol used with this prototype requires that the sensor module to be removed after calibration and reinserted for measurement. This results in small changes in the position of the sensor with respect to the electromagnet, also causing changes in the polarization field strength that is measured by the sensor. To correct for these effects, the reference signal generated by the

first element in each row is recorded by the software and averaged over the array. The array is scanned multiple times and the electrical signal sent to the electromagnet is adjusted after each pass to maintain a constant polarization field strength. The results from the scans are averaged to further improve the SNR.

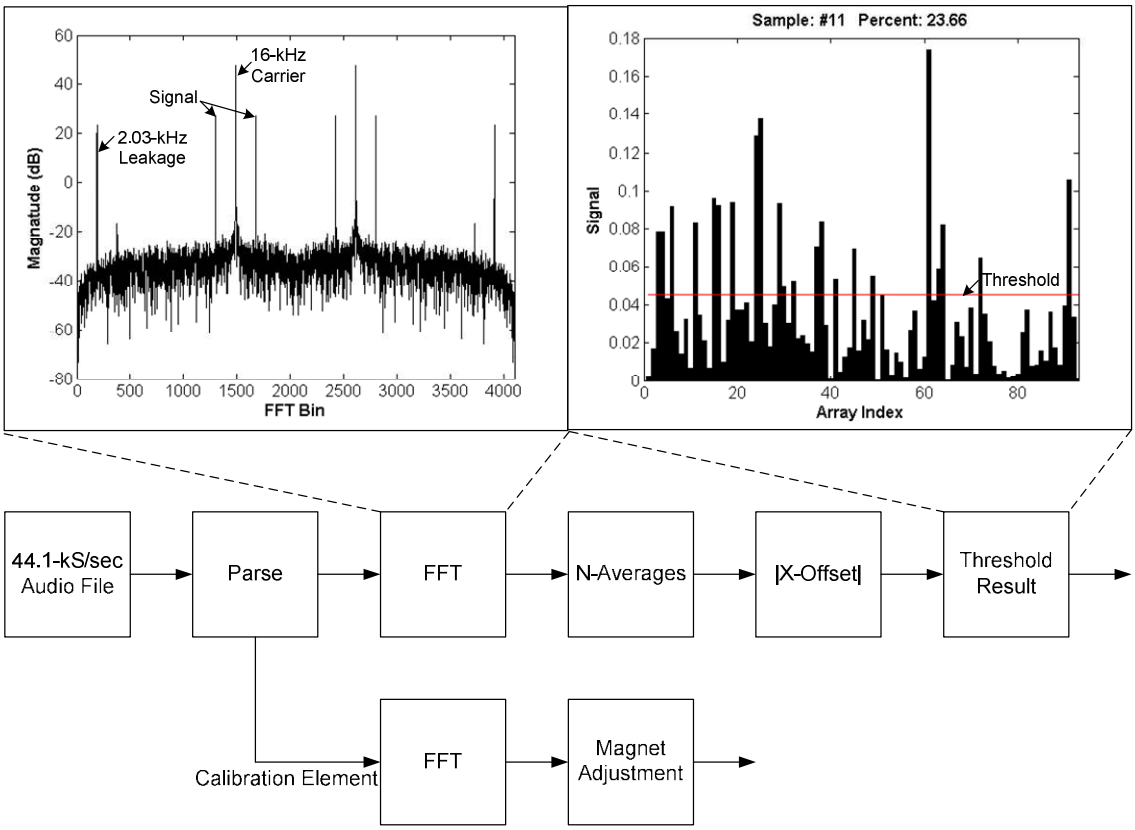

Figure 2.12: Summary of software functions, with example FFT output (top left) and final output (top right).

2.8.2 Software Design

Figure 2.12 shows a summary of the software functions. Detailed software code is included in Appendix B. The primary function of the software is to measure the signal

power levels at 16 kHz +/- 2.03 kHz, which corresponds to the upconverted signal from the magnetic bead. To achieve this, the sensor output is sampled at 44.1-kS/sec, and data is stored in an audio file. This file is run through a parsing algorithm to separate responses from each element in the sensor array. This algorithm uses energy detection within a window in order to identify the start of valid data, and then parses the remaining content according to preset constants. Next, a Hamming window is applied before the 4096-point FFT is taken and the energy in bins at 16kHz +/- 2.03kHz are added. The first output in each row (array index 1, 33, 65,…) is extracted and used for normalization and electromagnet level control. The process is repeated and the results for a particular array index are averaged. Next, the baseline (no bead, absolute value) response is subtracted from the signal (absolute value), and the resulting value is compared against a threshold. The threshold is determined based on the noise level of the system, so that less than 1% false detection occurs when no beads are on the sensor surface. Due to variation in the position of a bead in reference to a sensor element, the signal measured by the sensor can vary significantly. For 5 samples from the assay in Section 3.2.3, the mean signal level from a bead was found to be 0.75 Gauss, with a comparatively large standard deviation of 0.3 Gauss. Signal levels as high as 1.8 Gauss were recorded.

2.8.3 System Performance

To determine the average uncalibrated polarization leakage, the baseline data from five modules was used. Note that this is not the direct leakage of the polarization signal to parts of the measurements system, but the upconverted leakage resulting from sensor device mismatch. The average uncalibrated polarazition signal leakage was found

to be 10 Gauss for the 35-kA/m polarization field, corresponding to an average device mismatch of 1.3%. This value is determined by intrinsic CMOS processing parameters and bias condition. After calibration, the average leakage signal was reduced to 0.1 Gauss (with electromagnet level adjustment) and 1 Gauss (without electromagnet level adjustment).

The noise level can be adjusted by changing the system noise bandwidth (NBW), and must be set to provide adequate a SNR for reliable detection of beads. The noise bandwidth is determined by the FFT and subsequent averaging. With a Hamming

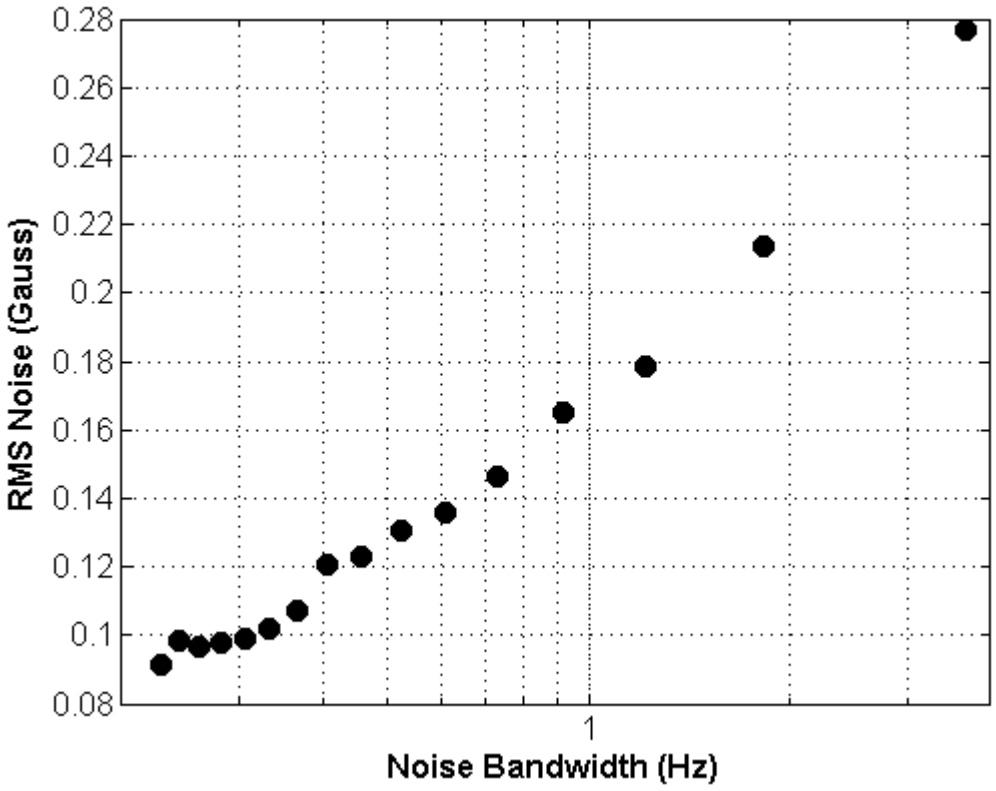

Figure 2.13: Measured RMS noise vs. noise bandwidth (NBW), for bandwidth from 0.23 Hz to 3.66 Hz.

Window and 4096-pt. FFT, the noise bandwidth is:

$$NBW = 1.36 \times \left({}^{44100}/_{4096}\right) \times \left({}^{1}/_{N}\right)$$

Here, *N* is the number of averages. Figure 2.13 shows the measured electrical noise level of the sensor for equivalent NBWs from 0.23 Hz to 3.66 Hz. The NBW was varied by adjusting the averaging number *N* from 4 to 64. For this work, N = 40 (NBW = 0.37 Hz). The total measurement time for the system is:

$$T = \frac{N \times \mathrm{M}}{8} \ (seconds)$$

where *N* is the averaging number, and *M* is the number of array elements read. For 1024 elements and N = 40, this corresponds to a measurement time of 85 minutes. Due to the long measurement time, a reduced number of array elements were measured for the assays in Chapter 3.

2.9 Design Summary

The use of a CMOS sensor array with adequate sensitivity for detecting magnetic beads has been validated. The low sensitivity of the CMOS Hall sensor requires that other negative phenomenon, such as polarization-signal leakage, are mitigated. Upconversion of the signal eliminates the primary polarization-signal leakage path, and improves the noise performance of the sensor. The use of a differential Hall sensor provides an additional 30 dB of leakage reduction. Still, the residual offsets of the CMOS devices are 20 dB larger than the bead signal. Offline calibration provides an additional 40-dB improvement. The use of offline calibration complicates the use the device.

However, the calibration described here could be done in advance, during manufacturing. This approach has been effective in a number of commercial products, but adds cost.

The linear indexing employed in the design allows for a simple analog interface for the sensor module. The complexity of data conversion is off-chip, simplifying the electronics on the sensor chip. The negative consequence of this approach is significantly longer read times. As described in section 2.8, reading all 1024 array elements with adequate SNR takes 85 minutes. This is probably excessive for most applications. In Chapter 3, assays were performed using fewer array elements, implying that a smaller array could be used for many applications. To reduce the read time further, two approaches could be employed. First, several array elements could be read out at the same time. Second, improvements in the SNR of the sensor device could shorten read times. This improvement could come from a different sensor design, and from optimization of system parameters such as polarization-field frequency and noise bandwidth. Finally, the distance between the bead and the sensor may be shortened by implementation or process changes. For example, CMOS process-node scaling typically results in the reduction of both the width and the thickness of metal layers, and a reduction in ILD thickness.

Chapter 3

Magnetic-Particle Assay (MPA) Platform Evaluation

3.1 Methodology

The primary requirement for a new diagnostic platform is that it produces clinically relevant results. The performance of a platform in a clinical environment is dependent not only on sensitivity and range of detection with respect to the target analyte alone, but also in the context of the clinical sample, such as blood, urine, or saliva. The evaluation is typically a multi-step process. First, benchmarks of absolute sensitivity and range of detection are evaluated with a purified-protein assay. The concentration of the target can be adjusted easily to evaluate the platform performance, and assay parameters can be tuned to balance sensitivity with range of detection. However, this type of assay has limited clinical relevance since only purified reagents are used, without the presence of other competitive or inhibitive molecules that may exist in a real sample. Next, the diagnostic platform is evaluated in comparison with a clinically relevant reference assay, using real clinical samples. This step may be repeated with different types of assays or targeting different diseases, in order to expand the applicability. However, in the case of the MPA platform, the similarities with standard ELISA allow some amount of extrapolation. In this chapter, the performance of the MPA platform is evaluated in comparison to ELISA in the context of two immunoassays: 1) the detection of purified protein antigen (mouse immunoglobulin) for sensitivity analysis and 2) the detection of

dengue virus-specific human IgG in serum samples to assess sensor function in a clinically relevant assay.

A secondary requirement for a new platform is verification that the clinically relevant results can still be achieved while providing benefits in protocol, ease of use, size, cost, etc. The process of improving the protocol, or reducing equipment size, can be time consuming, since verification of performance is continually required. In this chapter, the results presented correspond to baseline protocol and equipment. Possible optimization in protocol will be discussed at the end of the chapter.

The MPA platform is intended to benefit from existing assay development, particularly ELISA. The similarities between the biochemistry in ELISAs and MPAs can enable some amount of assay portability. For example, many of the assay components, such as reagent selection, can be reused in the MPA. Ideally, assays developed for ELISA can be quickly migrated to the MPA platform without much additional development. This feature may be significant for disease detection in regions with constrained resources, such as developing countries. An existing ELISA may be transferred to the MPA platform with little initial investment, and with potentially little highly skilled support.

3.2 Purified-Protein Assays

3.2.1 ELISA

The first assay to be evaluated detects mouse IgG using a sandwich-type structure. The purified mouse IgG protein concentration was varied by titration with PBS,

providing a controlled mechanism for evaluating assay sensitivity and range of detection. The detailed protocol is described in Appendix C.

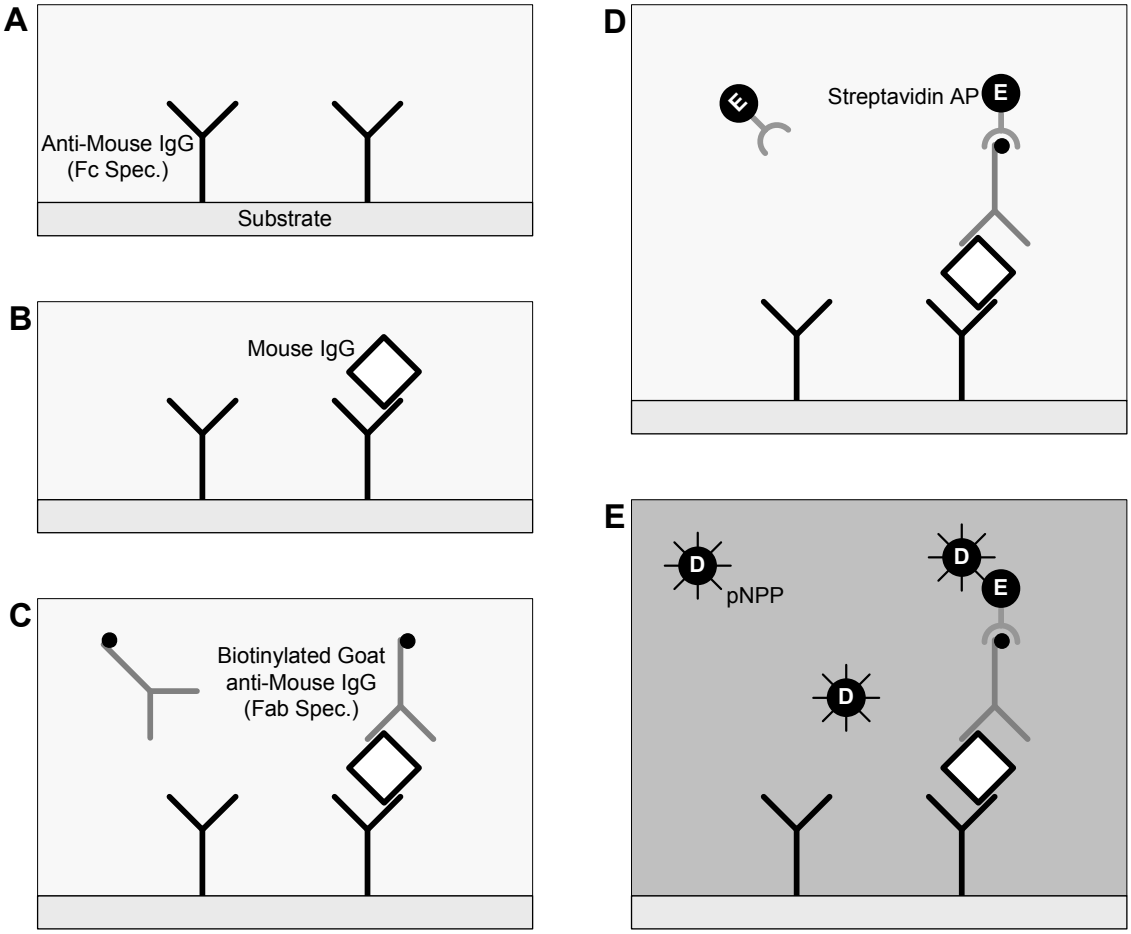

Figure 3.1: Simplified view of ELISA purified protein protocol, consisting of anti-mouse IgG coating antibody (A), mouse IgG target binding (B), biotinylated goat anti-mouse IgG secondary antibody (C), AP-conjugated Streptavidin (D), and catalyzation of nPP dye (E).

First, the polystyrene wells were coated with the capture antibody diluted in coating buffer (Figure 3.1A). Here, polyclonal anti-mouse IgG (Fc-region specific) was

used. This antibody was incubated overnight at 4 °C, so that it adsorbed onto the polystyrene surface. After incubation, the surface was washed with Phosphate-Buffered Saline and Tween solution (PBS-T) and then blocked with Non-Fat Dry Milk (NFDM), to prevent further adsorption of nonspecific proteins and thus minimize background noise during testing. Reference to numerous other washing steps that occur in this and other protocols in this chapter will be omitted in the remaining text, but are listed explicitly in the Appendices. It should also be noted that preparation up until this point in the protocol can potentially be done in advance of sample testing, assuming that coating proteins can be stabilized until testing takes place. Next, varying dilutions of mouse IgG were added (Figure 3.1B), and allowed to incubate for 16 hours. The incubation time must be chosen to balance assay sensitivity with protocol time. Incubation time can be significantly reduced with only marginal decreases in sensitivity, particularly if the temperature is raised closer to 37 °C. The concentration of mouse IgG was varied from 100 pg/ml to 1 μg/ml. Next, 0.2-μg/ml biotinylated goat anti-mouse IgG (Fab-region specific) was added (Figure 3.1C). Biotin is a small protein (~250D) with high avidity for streptavidin. The process of biotinylating an antibody usually does not affect its binding behavior. Next, 1.5-μg/ml streptavidin conjugated with the enzyme alkaline-phosphatase (AP) was added (Figure 3.1D). The use of a biotinylated secondary antibody and streptavidin-AP standardizes the biochemistry, and allows the streptavidin-AP to be shared generically across different assays. The direct conjugation of AP to the secondary antibody is less common than biotinylation because the high molecular weight (~100kD) of AP can affect the binding behavior of the secondary antibody. Finally, the dye p-nitrophenyl phosphate (pNPP) was added, and the reaction catalyzed by the enzyme AP (Figure 3.1E) was

allowed to proceed for 15 minutes in the dark. This resulted in a color change proportional to time course and amount of AP present, indirectly indicating the target analyte concentration. A quantitative color measurement was made using a spectrophotometer (Biotek Instruments, Winooski, VT), and the final assay output was Optical Density (O.D.).

3.2.2 Magnetic-Particle Assay (MPA)

The purified-protein mouse IgG ELISA can be ported easily to the MPA platform. In this section, two assays are described. The first assay utilized magnetic beads and the sensor module described in Chapter 2. The protocol is shown in Figure 3.2, and described in detail in Appendix D. In addition, a second assay was performed using magnetic beads that were counted by manually under a microscope. The optical count provided a simple cross-check to ensure that the sensor system was counting the number of beads on the surface accurately. In the transfer of the purified protein assay, the ELISA protocol was migrated almost directly, and no simplification was made to the MPA protocol. The first three steps (Figures 3.2A-C), are nearly identical to the ELISA protocol. The only notable difference is that the substrate contains the integrated magnetic sensor, covered by a thin gold layer. As noted in Chapter 2, the adsorption properties of gold are similar to those of polystyrene, so that no change in incubation time or coating buffer was required. However, the continued use of a biotinylated secondary antibody has less obvious benefits in the MPA platform. Magnetic beads can be coated with almost any protein, and can be viewed as a second substrate. There are two primary reasons that the biotinylated secondary antibody was used in conjunction with streptavidin coated magnetic beads.

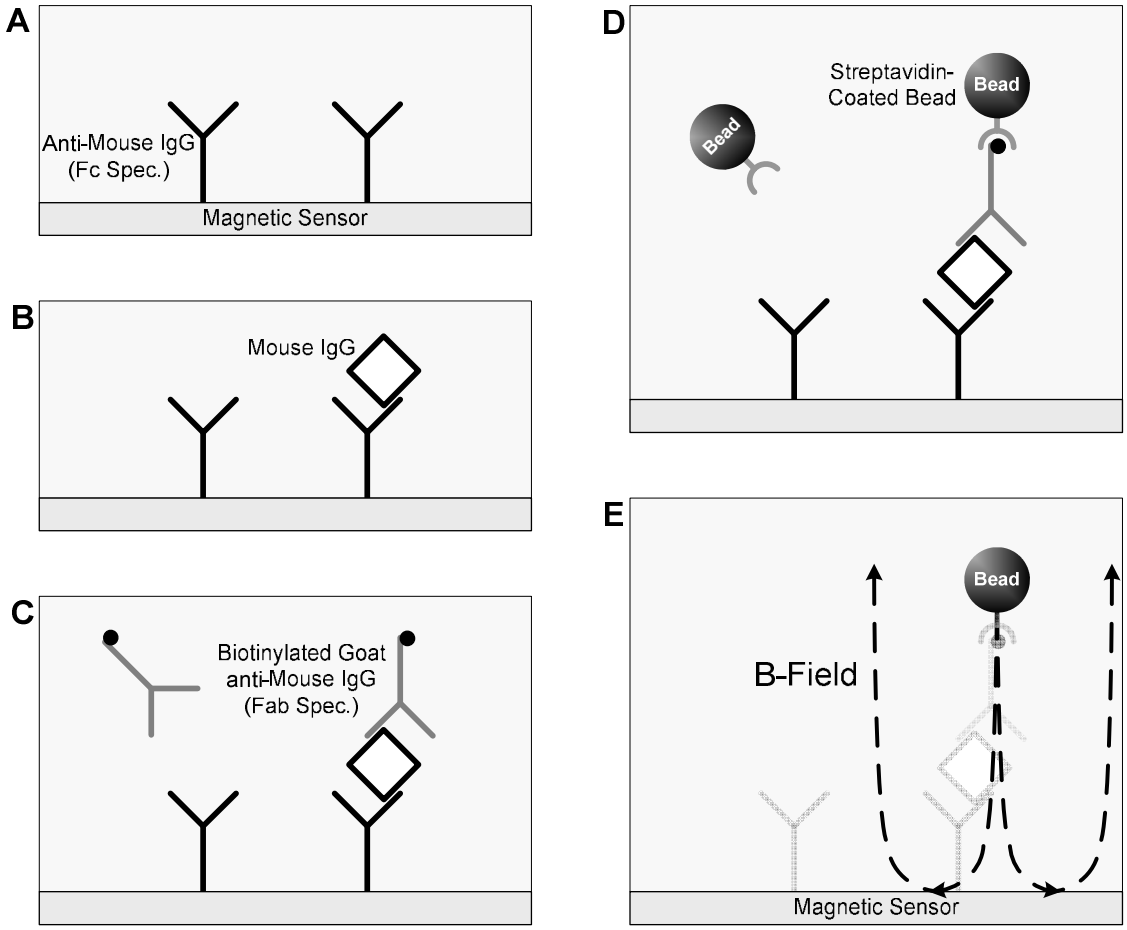

Figure 3.2: Simplified view of MPA purified protein protocol, consisting of anti-mouse IgG coating antibody (A), mouse IgG target binding (B), biotinylated goat anti-mouse IgG secondary antibody (C), streptavidin-coated magnetic beads (D) and their detection by the sensor (E).

First, preserving this structure allowed more direct comparison of the MPA platform and ELISA. Second, many types of magnetic beads are available coated with streptavidin and the bead surface is blocked by the bead manufacturer. The process of blocking the bead surface is dependent on the bead construction and is often proprietary, making it impractical outside of the manufacturing environment. In the fourth step of the assay,

streptavidin-coated magnetic beads (2-20-μm poly-dispersed, 90% magnetite, Polysciences), diluted 1:100 in PBS-T, were added (Figure 3.2D). The selection of these beads was motivated by their high magnetite concentration. However, this choice had some negative effects on other aspects of the assay, and other beads were subsequently used. The optical detection assay used smaller, mono-dispersed beads (3-μm, 15% magnetite, Seradyn). The trade-offs in bead selection will be discussed later in the chapter. After adding the beads, excess and non-specifically bound magnetic beads were removed by magnetic washing. In this protocol, a permanent magnet was used for magnetic washing. The magnetic washing step in the MPA protocol is significantly different from the liquid washing steps in the ELISA protocol. The strength of the magnetic field can be adjusted, so that the force applied to the magnetic beads can be adjusted. To optimize the magnetic washing, permanent magnets of various sizes were applied for time intervals and different distances from the detection surface. Incremental increases in the washing force (based on a larger magnet, longer time period, and shorter distance) were applied to a 1 μg/ml sample and a 0-μg/ml sample, and the washing force was considered optimized when the ratio of bound beads for the 1-μg/ml sample to bound beads for the 0-μg/ml sample was greatest, thereby maximizing the potential dynamic range of the assay. The optimal magnetic washing was found to be with a 5-mm barrel-type rare-earth magnet placed in contact with the top of the microtiter fluid for a period of 30 sec. The bottom surfaces of the microtiter wells were visualized under bright-field with a 20X objective lens using a microscope. Three random fields were counted for each well, and the number of beads was averaged at each protein concentration. After washing, magnetic beads that remained bound to the sensor surface were detected by the

magnetic sensor (Figure 3.2E), indirectly indicating the analyte concentration. As discussed in Section 2.8.2, the software outputs the fraction of array elements that generated a positive (above threshold) signal. The MPA output of 'Percent' can be compared with the ELISA output O.D. through a scaling factor. An example of this output is shown in Figure 3.3.

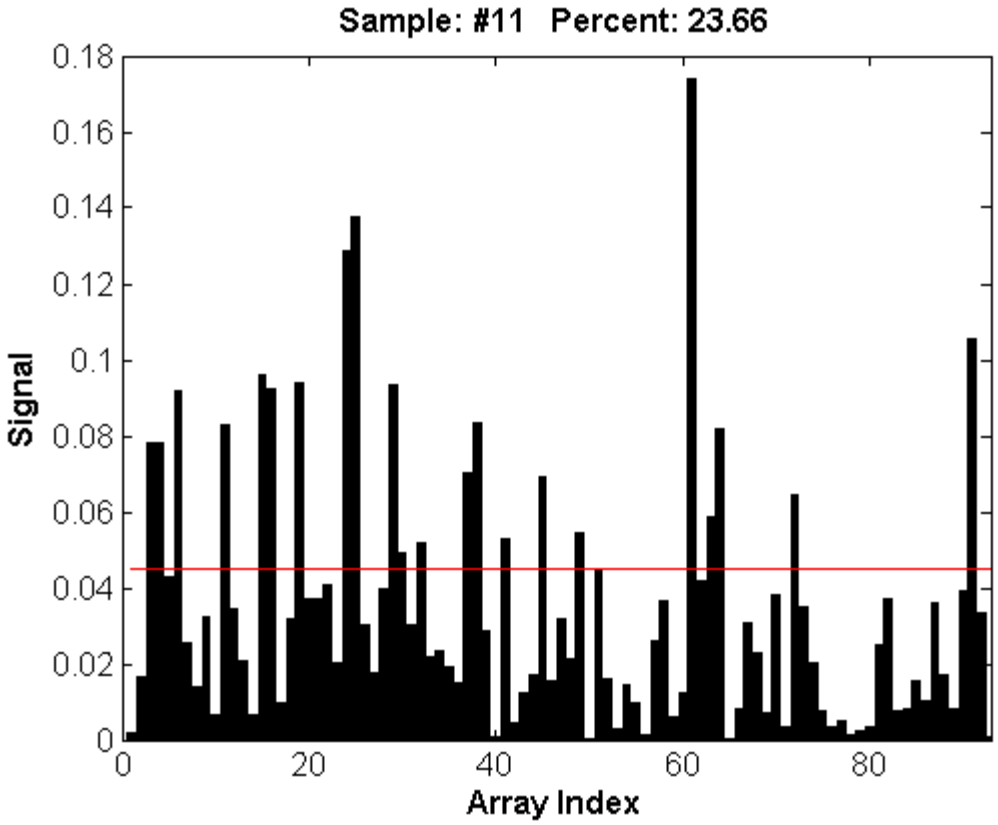

Figure 3.3: Example MPA platform software output, including sample name (top left) and assay result (top right).

3.2.3 Platform Comparison

The sensitivity and range of detection was evaluated for ELISA, MPA using optical (visual) evaluation of bead count, and MPA using the integrated sensor and counting

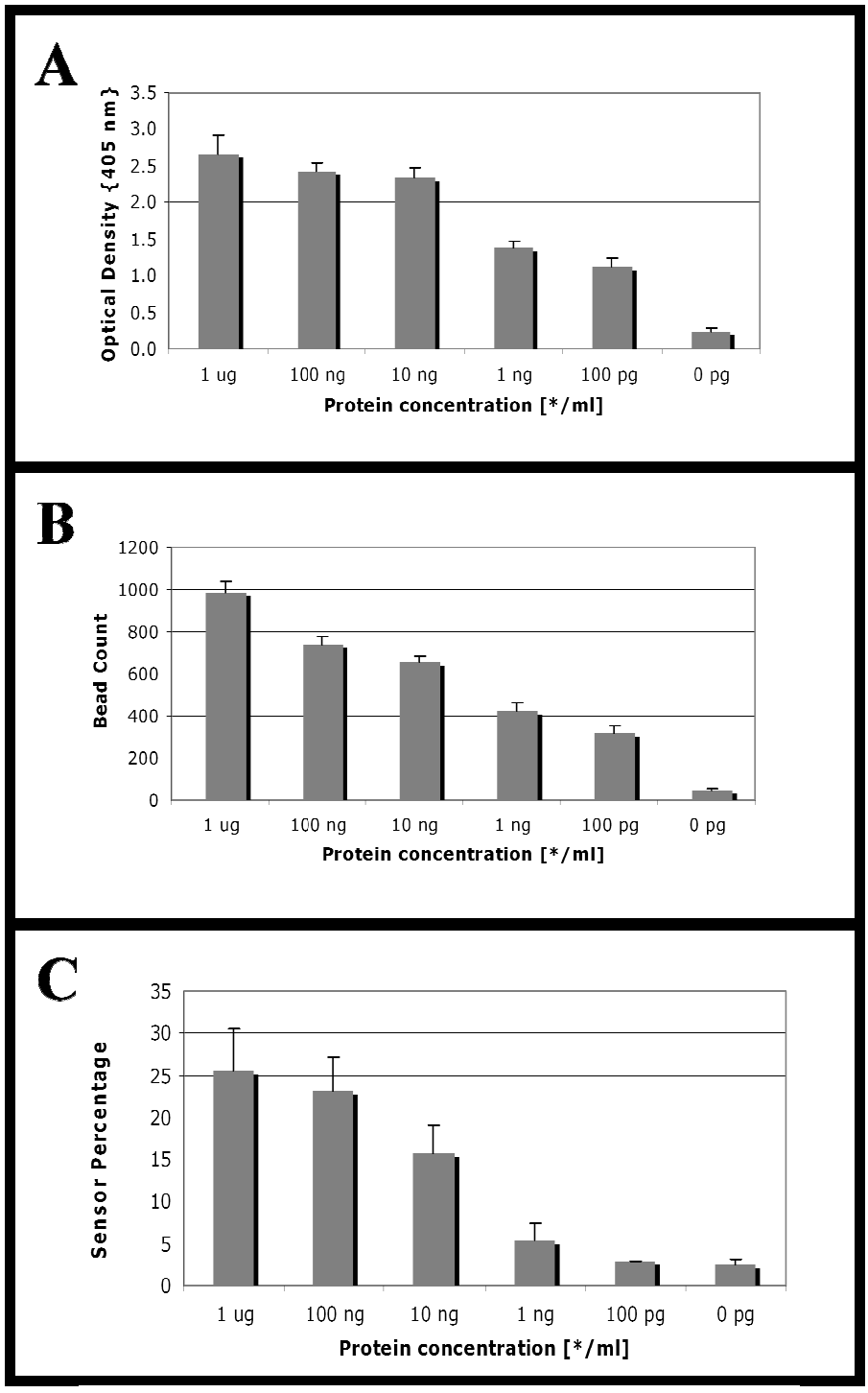

Figure 3.4: Purified-protein results for ELISA (A), MPA using optical counting (B) and MPA using sensor detection and counting (C).

methodology as described in Chapter 2. The results of all three approaches are shown in Figure 3.4. In the microtiter wells, detection was performed with streptavidin-AP and pNPP substrate for ELISA as well as streptavidin-coated beads magnetically washed with a permanent magnet and then counted under 200X magnification. The sensor wells were washed with the same permanent magnet, and detection was performed by placing the sensor well in the reader, where the results were reported as the percentage of sensors with a signal magnitude exceeding the detection threshold (as described in Chapter 2). The ELISA and the magnetic bead on microtiter wells demonstrated a detection sensitivity of 100 pg/ml whereas the sensor detected beads at 1 ng/ml (Fig 3.4). Note from Figure 3.4B that the magnetic bead count displays a log-linear dependence on concentration. The discrepancy between the optical (Fig. 3.4B) and sensor (Fig. 3.4C) magnetic bead quantitation results may be due to the use of the larger high magnetite beads in the sensor assay, which are suboptimal for magnetic washing. Larger beads are easily pulled from the surface, while smaller beads require more washing force. In addition, some of the larger beads show evidence of "clumping". This results from the magnetic remnance in the beads, which is larger for larger beads. Finally, the use of a permanent magnet for magnetic washing makes the process less repeatable. The centerline of the magnet may change to with respect to the sensor, altering the results.

3.3 Serum Assay for the Detection of Dengue Virus

3.3.1 Background

The detection of an infectious disease in a clinical setting can be accomplished through direct detection of the disease itself (antigen detection), or by indirect indication

provided by an immune response (antibody detection). Direct detection has the advantage that it can be measured immediately, without waiting for the patient to generate an immune response. However, the concentration of the disease agent itself may be small and below the sensitivity of the assay. Indirect detection relies on measurement of antibodies produced in response to the disease. The type of antibody can also indicate the time frame of the infection, and whether the patient has had the same disease in the past. IgM antibodies are generally present early in an immune response. However, they are of lower specificity than other antibodies. Low antibody specificity may translate into lower assay sensitivity. This can occur when an antibody demonstrates some binding affinity for another antigen, leading to an increase in false signals or background. IgG antibodies occur later in an immune response, or when the patient has had the same infection in the past. These antibodies have high specificity and can result in more sensitive assays. In practice, more than one assay may be required to balance the need for early and reliable detection.

In this section, an assay for detection the dengue virus is considered. Dengue is a widespread infectious disease spread by mosquitoes, and is in the same family as West Nile and Japanese Encephalitis. Dengue is prevalent in over 100 countries worldwide, including Central and South America, Southeast Asia, and India. In many areas, adequate medical facilities for reliable diagnosis are not available. In some cases, samples must be sent hundreds of miles for processing in a centralized national laboratory. This results in significant costs and delays that make widespread monitoring and detection of dengue difficult. The detection of IgG against dengue has been shown to be clinically relevant, and was selected for comparison of ELISA and MPA, using serum as the starting

material. Serum is extracted from whole blood by centrifuge, which may not be readily available in some clinical environments. Recently, an assay that uses saliva as starting material has been presented (Balmaseda et al., in prep.). Saliva is an attractive alternative to serum, since no additional processing of the sample is required and sample collection is typical easier.

3.3.2 ELISA

Figure 3.5 shows an overview of the ELISA, which uses an antibody-detection format. The detailed protocol is described in Appendix E. The polystyrene well was coated with dengue virus antigen prepared from the four serotypes (DENV1-4), diluted to a concentration of 70 mg/ml, and incubated overnight (Figure 3.5A). The use of all four serotypes in the coating antigen is required for complete coverage, since patient serological information is not known in advance. The wells were washed with PBS-T and blocked with NFDM. Next, diluted serum was added and allowed to incubate overnight (Figure 3.5B). The serum was collected from patients in Nicaragua, and had been previously tested using a similar assay. Patients with dengue, or who have had dengue in the past, will have IgG against dengue virus present in the serum. This IgG binds specifically to the dengue-virus antigen. The remaining serum was removed by washing with PBS. Next, 0.2-μg/ml concentration biotinylated goat anti-human IgG was added and allowed to incubate for 1 hour (Figure 3.5C). Excess is removed by washing. The remaining steps (Figures 3.5D,E) are the same as in the purified protein assay.

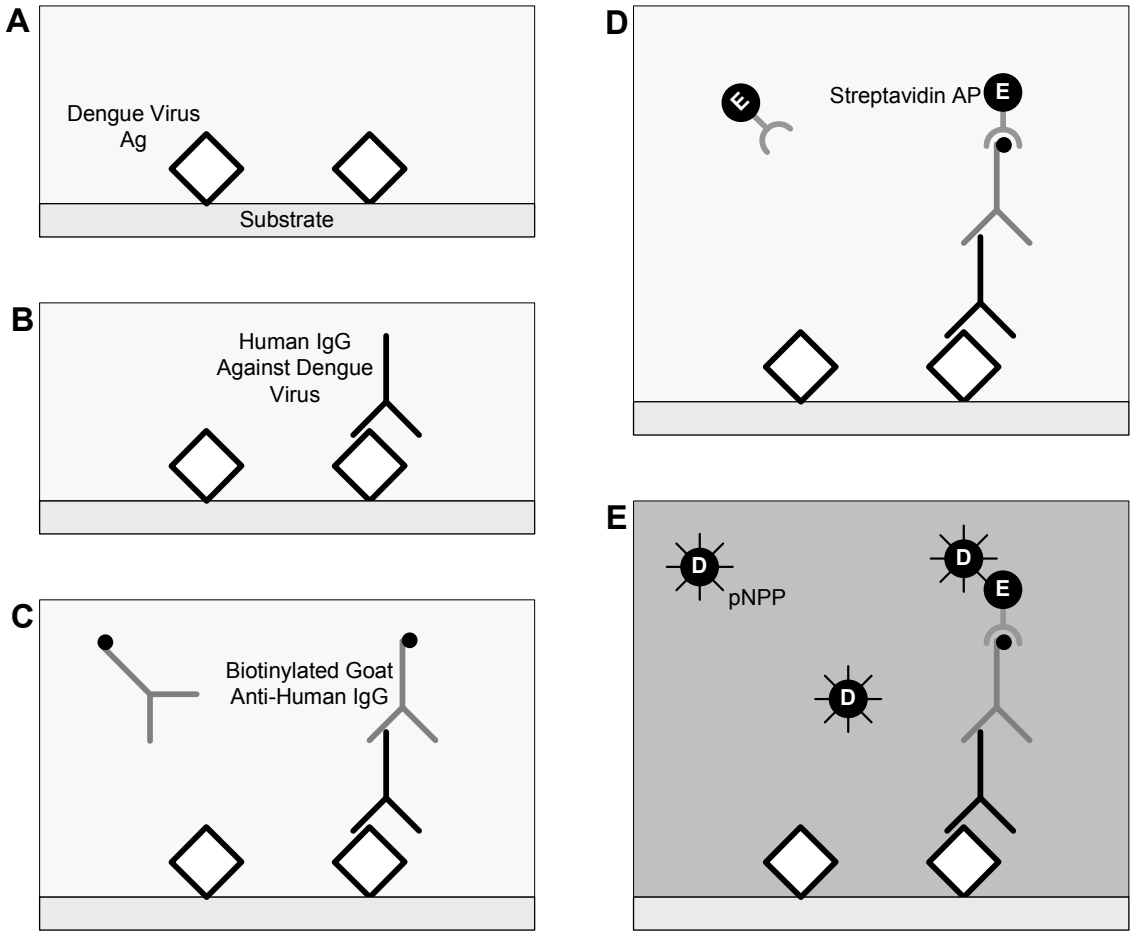

Figure 3.5: Simplified view of ELISA purified protein protocol, consisting of dengue-virus coating antigen (A), anti-dengue virus human IgG target (B), biotinylated goat anti-human IgG secondary antibody (C), AP-conjugated Streptavidin (D), and catalyzation of nPP dye (E).

3.3.3 Magnetic-Particle Assay (MPA)

Mapping of the serum ELISA to the MPA platform is similar to the purified protein assay, as shown in Figure 3.6. A detailed description of the protocol can be found in Appendix F. Two distinctions exist from the purified-protein MPA in Section 3.2. First, 4.1-μm monodispersed magnetic beads (15% magnetite, Spherotech) were used.

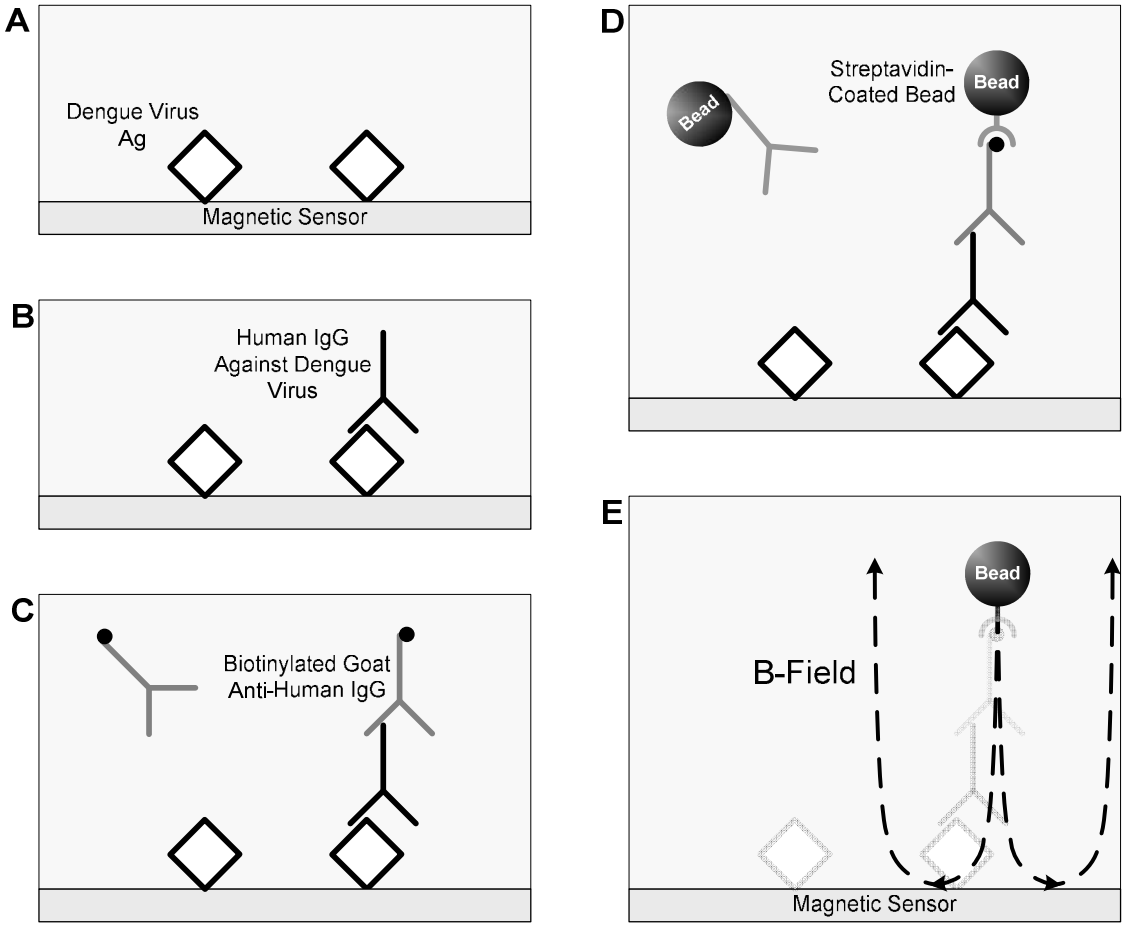

Figure 3.6: Simplified view of serum MPA protocol, consisting of dengue-virus coating antigen (A), anti-dengue virus human IgG target (B), biotinylated goat anti-human IgG secondary antibody (C), streptavidin-coated magnetic beads (D) and their detection by the sensor (E).

Second, magnetic washing was implemented using an electromagnet and a DC power supply. For magnetic washing, the electromagnet was powered by a manually adjusted DC power supply and was modified with a removable adaptor that was placed in the electromagnet gap directly under the biosensor, as described in Chapter 2. The washing force was optimized by incrementally increasing the applied field and gradient from

approximately 390 Gauss with a gradient of 211 Gauss/cm to 470 Gauss with a gradient of 560 Gauss/cm. Incremental increases in force were applied to sensors that had been incubated with either a positive or a negative serum sample and then measured. The washing force was considered optimized when the ratio of the sensor percentage for the positive serum sample to the sensor percentage for the negative serum sample was greatest, thereby maximizing the potential dynamic range of the assay. The optimized washing force for the detection of anti-dengue virus IgG in serum was found to be 450 Gauss with a gradient of 460 Gauss/cm applied for 30 sec. The sensor measurement commenced within 2 minutes of washing. The normalized covariance was calculated using the *corrcoef* function in Matlab and used as a criterion for correlation between the two assays.

3.3.4 Platform Comparison

To evaluate the sensor chip in a clinically relevant assay, 12 clinical serum samples from persons suspected of dengue virus infection were tested for the presence of IgG antibodies against dengue virus antigens using the sensor chip assay compared to ELISA. The ELISA protocol was transferred to the sensor chips with minimal modification in order to provide a direct comparison between the sensor chip and ELISA results. The magnetic bead sensor assay data (% positive) and the ELISA results (in OD) are shown in Figure 3.7. A strong association was observed between the two assays, with a R^2 of 0.966. The 4.1-μm mono-dispersed magnetite beads function significantly better for magnetic washing than the poly-dispersed beads, and provide consistent recognition by the sensor elements.

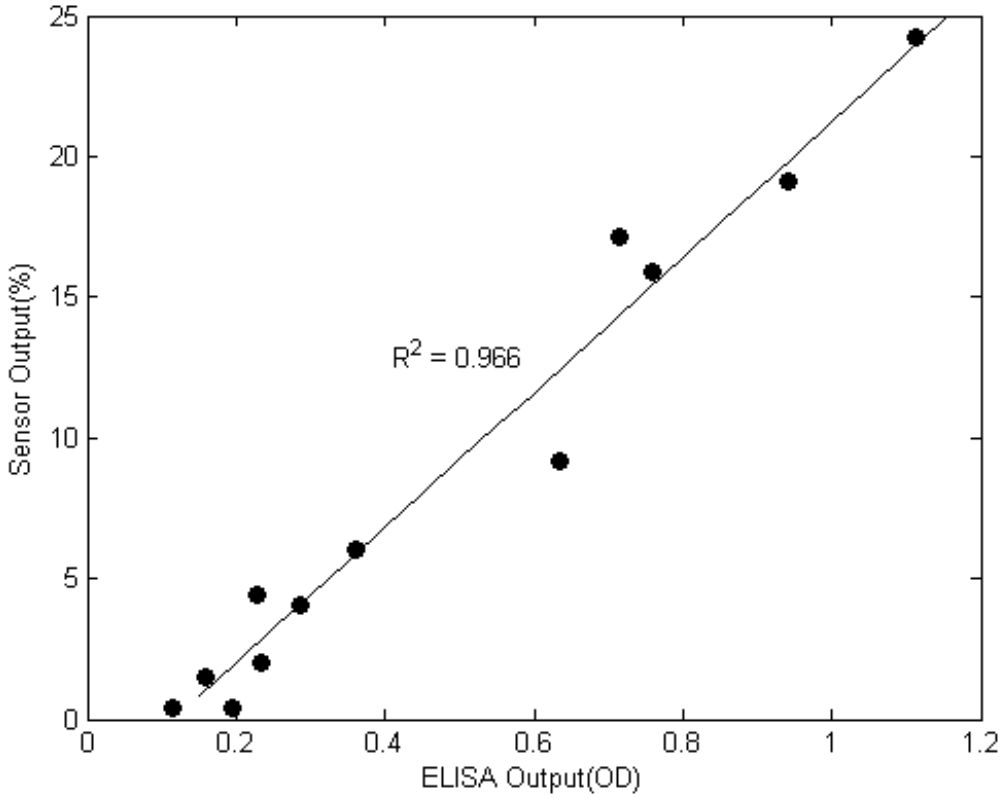

Figure 3.7: Correlation between MPA sensor output and ELISA OD, using serum samples from 12 patients.

The potential dynamic range of these assays can be estimated by calculating the ratio of the output from the highest positive serum sample (% Positive or OD) to the lowest negative serum sample (% Positive or OD). The higher this signal-to-background ratio is for a particular assay, the greater the potential of the assay to provide a distinct output across a wide range of input analyte concentrations. For the detection of human IgG against dengue virus in our clinical serum samples, this ratio was found to be 16 for the sensor assay and 7 for the ELISA.

3.4 Assessment

3.4.1 Magnetic-Particle Assay (MPA) Protocol and Correlation

The correlation between the MPAs detecting either protein antigen or serum antibody against a pathogen with their respective ELISAs is encouraging evidence for clinical validity. The similarity in biochemistry between MPA and ELISA suggests that comparable results may be achievable in other immunoassays, and that a broad range of diseases currently detectable by ELISA are also detectable using the MPA. This high correlation between ELISA and MPA platforms was achieved with a protocol that was identical wherever possible. However, the selection of beads and magnetic washing parameters are unique to the MPA platform, and will require continued development work for a particular assay.

In addition, strict adherence to the ELISA protocol can preclude simplifications and optimizations that otherwise would be possible on the MPA platform. One goal of the MPA platform is to enable disease detection in environments where ELISA is impractical, such as small clinics in developing countries. In these areas, purified water that is required for liquid washing steps may not be available. Therefore, deviating from the ELISA protocol may be required in order to make the assay practical. To reduce the number of reagents used, the magnetic beads can be coated with the appropriate secondary antibody, rather than streptavidin. This will eliminate the need for a separate biotinylated secondary antibody. To reduce or eliminate liquid washing, some significant changes to the MPA protocol are likely to be required. For example, magnetic beads may be premixed with the sample, allowing the beads to serve as a second substrate. Since the beads are magnetic, they may be moved from the original sample to the measurement

area by magnetic manipulation. Local magnetic fields have been used to manipulate beads on a sensor surface (Tondra et al., 2005). Thus, one or more local magnetic fields could be integrated into the reader, providing improved bead handling for enhanced mixing and binding to the sensor surface (Gijs, 2004). The protocol then may resemble the combination of common magnetic separation techniques (Safarik and Safarikova, 2007) and the measurement portion of the MPA.

3.4.2 Magnetic Bead Selection

Magnetic beads from numerous manufacturers were investigated with respect to use in magnetic washing and sensor detection. Many bead characteristics, including mean diameter, size, and magnetite concentration, impact assay performance. Beads with diameters less than 1.5 μm demonstrated vibration due to Brownian motion in fluid even when specifically bound to a surface, contributing an additional component to electrical noise and making them unsuitable for sensor detection. Furthermore, bead settling is required for the beads to be captured on a surface. Larger beads and those with higher magnetite content were found to settle more quickly. For best results with magnetic washing, mono-dispersed beads gave better results than poly-dispersed beads. The 3-4-μm, 15% magnetite beads resulted in the best combination of uniform reliable magnetic washing and sensor detection. Finally, beads from Chemagen AG (Baesweiler, Germany) appeared to not be blocked effectively. This resulted in beads binding to the sensor surface even when the target protein was not present. This phenomenon was not observed with other beads.

A preliminary investigation into the complex susceptibility was also conducted. A sample was measured with polarization field frequencies of 872 Hz and 2.024 kHz. Magnetic beads (2.6 μm, 15% magnetite, Seradyn) were dried on the surface to prevent any movement between measurements. The polarization field of 25 kA/m was matched at each frequency by tuning. Figure 3.7 shows the response for both polarization field frequencies, and indicates a 2.3X increase in the average positive bead signal for the 872-Hz polarization versus the 2.024-kHz polarization. It should be noted that the beads and polarization field are smaller than those used in earlier simulation or measurement. Nevertheless, the data indicates that higher polarization-field frequencies may reduce the signal from a bead. Additional experiments should provide further information on

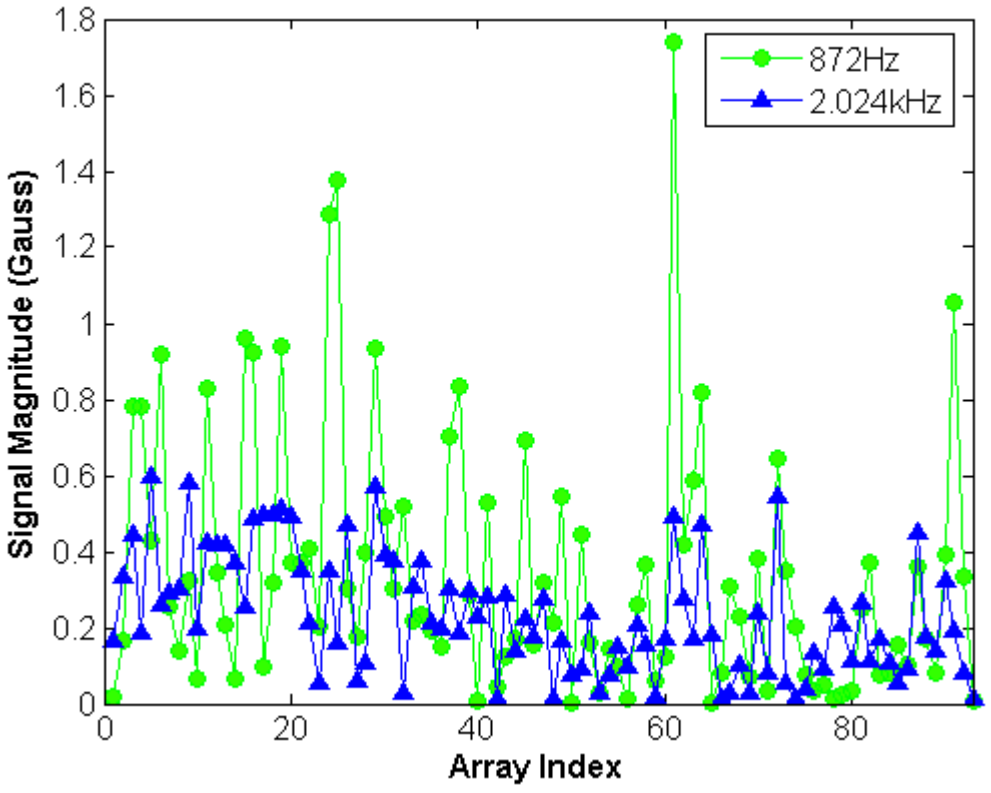

Figure 3.7: Sensor signal magnitude versus array index for two polarization frequencies, 872 Hz and 2.024 kHz, taken from the same sample.

frequency response and dependence on bead parameters, such as diameter and magnetite concentration.

The measured signal from a magnetic bead can be estimated from statistical analysis of the sensor array data from the MPA serum assay. The mean (0.75 Gauss) of the bead signal was estimated by averaging positive values from 5 sample assays. The expected value of the signal can be calculated by combining the data from Figures 2.1 and 2.4, and the array pitch information described section 2.3. With this approach, the expected value of the average signal from a bead on the array is found to be about 25% of the peak value (16 Gauss), or 4 Gauss. If the frequency response of the bead is also considered, this expected value is reduced to 1.7 Gauss. The measured value of 0.75 Gauss is lower, indicating an error in the bead signal modeling. The large variation in positive signals in the measured samples suggests that bead position with respect to a particular sensor needs to be modeled more accurately. For example, beads at the intersection of four array elements may be measured by all four, but with a reduced signal level. Two-dimensional image-processing algorithms may be required to detect these cases.

3.4.3 Magnetic Washing

Magnetic washing is an important component of the MPA platform. Initial methodology that used hand-held permanent magnets was prone to variability and requires good hand coordination. The reconfiguration of the primary electromagnet for application of the magnet washing field resulted in better results, excellent repeatability,

and no special skill. Furthermore, the control of the magnetic field by a precision current source allows the field to be easily adapted for different magnetic bead and assay requirements. In all magnetic washing protocols described in this chapter, the excess beads were physically removed from the sample well after washing. This is an inconvenient step that may not be required, since the measurement takes place only at the sensor surface. Magnetic beads could be pulled from the sensor surface but left in solution during measurement. This approach was evaluated on the prototype platform. First, the DC magnetic field was applied for washing. The system was quickly reconfigured, and the AC field was applied for measurement. However, due to the long measurement time in the prototype system, beads would resettle during the measurement. This resulted in high background for negative samples, and the approach was abandoned. Refinements in design, such as significantly shorter measurement time, may make this approach possible.

Chapter 4

Overall Platform Assessment

An assessment of the MPA platform based on this work can be broken into three components: viability of CMOS implementations, application benefits, and clinical validity.

4.1 CMOS Sensor

The viability of CMOS as a sensor for this application has been largely demonstrated. With appropriate design choices and calibration algorithms, the system delivers adequate sensitivity in order to achieve acceptable results at the platform level.

Some parameters, such as measurement time, will need improvement for most real-world deployments. However, a number of low or moderate-risk changes can be made to improve the measurement time. First, as described in Chapter 2, more sensors can be read simultaneously. Second, a higher sensitivity and lower noise sensor topology (such as NWELL) can allow an increased noise bandwidth and still provide reliable detection. In addition, optimization of platform parameters may improve SNR. Third, a reduced number of sensor elements may be acceptable for many applications. The sum of these improvements can be expected to reduce measurement times to less than 1 minute.

The calibration techniques developed in this work enables large reductions in significant technological hurdles, such as polarization field leakage and CMOS device offsets. The reduction of these effects was essential due to the intrinsically low sensitivity of the CMOS sensor. However, calibration may also present limitations in applicability,

by either increasing cost during manufacturing or complicating protocol in the field. The feasibility of eliminating the calibration requirement is less clear. Nevertheless, calibration is a viable solution technically and is probably acceptable in many applications.

4.2 Application Benefits

In addition to a valid clinical output, a successful detection platform directed at diseases in developing countries must also provide improvement in cost, portability, and ease of use. When compared with quantitative ELISA, the MPA platform demonstrated in this work has some intrinsic benefits for point-of-care or constrained-resource applications. The disposable prototype sensor and reusable reader, with the exception of the custom-made electromagnet, were developed and built using mass-production technology and contract manufacturing common in the electronics industry. This should lead to lower platform costs due to economies of scale, when compared to lower volume manufacturing techniques. Though the specific setup used for this work had large components (such as the audio amplifier), these parts are also commercially available in a more compact form and are significantly smaller and less expensive than a spectrophotometer system. Therefore, it is also reasonable to conclude that the reader system can be made for point-of-care or resource-constrained applications.

Another goal of this work was to provide a simple and automated assay protocol. This was not directly achieved, and the simplification and automation contains significant risk. In Chapter 3, the MPA protocol was intentionally similar to the ELISA protocol, allowing direct comparison of results. To simplify the MPA protocol, a number of

possibilities exist. First, a reduction in measurement time may allow beads to be left in solution during measurement. As noted in Chapter 3, measurement immediately after magnetic washing may be feasible if the measurement time is short enough.

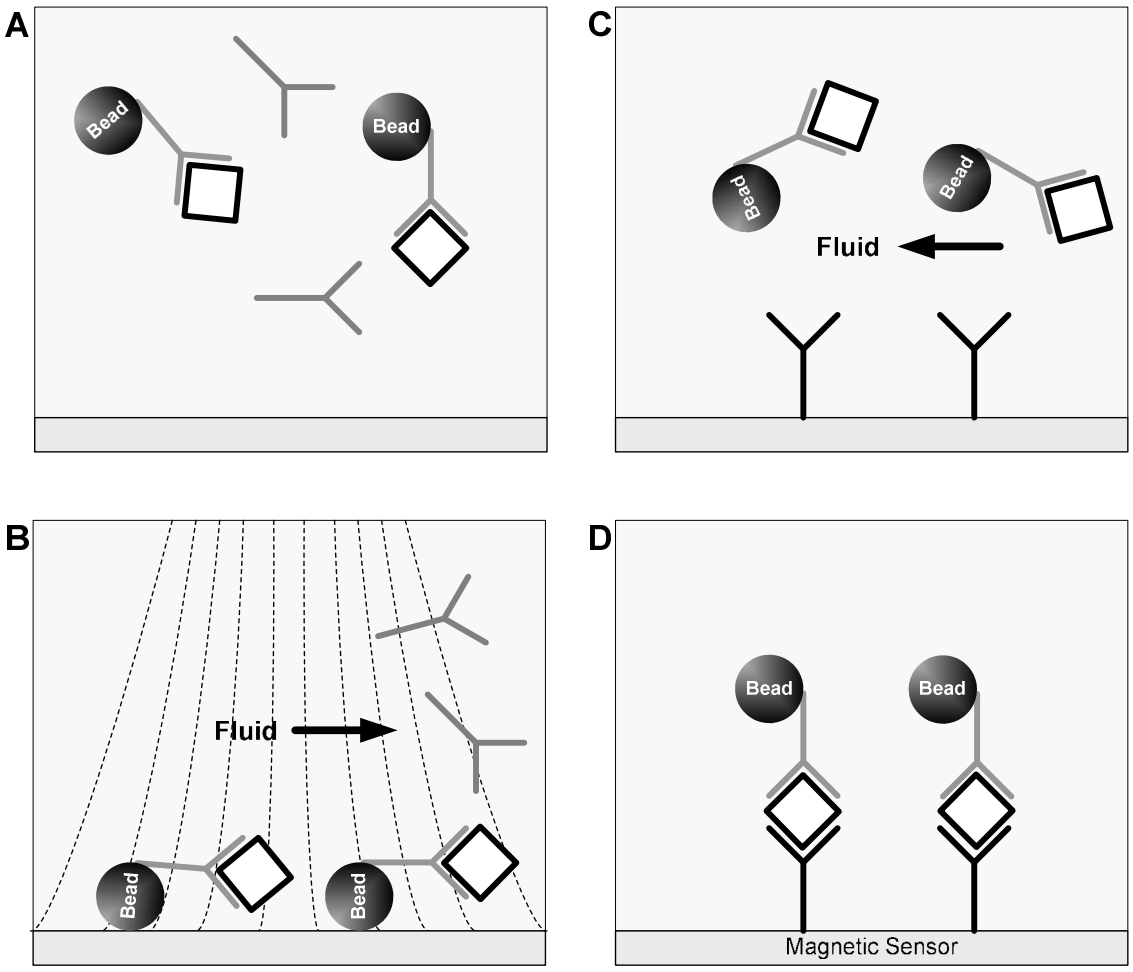

Figure 4.1: Combining magnetic separation with detection, by premixing beads with the target (A), immobilizing beads while flushing residual sample (B), introducing beads into the detection area (C), and measuring the beads after binding specifically to the coating protein (D).

Second, a magnetic separation may be employed prior to detection. This concept is shown in Figure 4.1. Initially, beads are mixed with the sample in order to capture the target protein (Figure 4.1A). Next, beads are held in place by a magnetic field while the liquid sample is removed and replaced with a clean solution (Figure 4.1B). Here, the surface that makes contact with the bead should be Teflon or something similar, so that the beads release easily. The beads are then re-suspended and moved to the sensor area (Figure 4.1C). Finally, they are allowed to bind with the sensor substrate, washed magnetically, and then measured (Figure 4.1D). This concept relies more on micro-fluidics, which may add cost and complexity. Nevertheless, more aggressive approaches are most likely required in order to achieve a simple, automated protocol that operates directly on clinical samples, such as whole blood, without pre-processing. In addition, systems will benefit from top-down design, where micro-fluidics, detection, and sample preparation are considered from the outset.

4.3 Clinical Validity

Chapter 3 provided encouraging data for the MPA platforms performance when compared with two ELISAs. The high correlation shown between the MPA and ELISA in the context for a real-world assay for the detection of dengue is a compelling starting point. Though more assays should be benchmarked on the MPA platform, these initial results, coupled with the similarities with ELISA in assay format and chemistry, are reasonable grounds for optimism in other immunological assays. As described in the introduction, immunological assays play a major role in the detection and monitoring of infectious disease.

In addition to immunological assays, other work has shown the MPA platform can also be effective in nucleic acid assays (Edelstein et al., 2000). The versatility of the gold sensor surface for biological assays is demonstrated by its capacity for passive protein absorption (Anwar et al., 2005), as well as its ability to be easily modified with thiolated oligonucleotides that facilitate the capture of target nucleic acids (Herne and Tarlov, 1997). Other efforts related to this project demonstrated the ability to capture an oligonucleotide sequence on gold surfaces and the use of a magnetic bead label to detect the captured sequence (J. Foley, T. Aytur, B. Boser, E. Harris, P. R. Beatty, unpublished data).

In summary, early but significant data points exist from this and other work that show the MPA as a flexible platform capable of addressing a range of clinically relevant problems in the detection and monitoring of infectious diseases.

4.4 Next Steps

There are a number of promising directions for future work on CMOS-based MPA platforms. First, refinements in the sensor and chip architecture should yield substantial benefits in test time and ease of use. In addition, the refinements could be combined with other technologies, such as microfluidics, in order to realize a more complete system for processing samples and outputting results. Ideally, no further handling of a sample would be required after initial collection, with all intermediate steps of the protocol performed by the test platform without operator intervention. However, additional technological complexity should not come at the expense of size or cost.

Beyond the improvements from engineering development, perhaps the most essential work will involve improvements in protocol simplicity. The potential of the MPA platform is largely unrealized until protocol simplification is demonstrated. Though significant engineering advances may also help simplify the protocol, many ideas can be tested without changing the existing platform. The use of macroscopic equipment, such as commercial magnetic separators, is a fast and technically reasonable path for investigating promising avenues. Success in this context would then motivate development of more advanced systems with appropriate size and cost parameters, and move the MPA platform closer to meeting the need of diagnosing and detecting infectious diseases.

Bibliography

Anwar, M.A., Aytur, T., Foley, J., Beatty, P. R., and Boser, B., 2005. Integrated circuit and micro-fabrication compatible materials for protein patterning. Proceedings of Micro Total Analysis Systems. 2005.

Balmaseda, A., Guzman, M.G., Hammond, S., Robleto, G., Flores, C., Tellez, Y., Videa, E., Saborio, S., Perez, L., Sandoval, E., Rodriguez, Y., and Harris, E., 2003. Diagnosis of dengue virus infection by detection of specific immunoglobulin M (IgM) and IgA antibodies in serum and saliva. Clin Diag. Lab Immunol. 10, 317.

Balmaseda, A., Saborio, S., Tellez, Y., Mercado, J.C., Pérez, L., Rocha, C., Kuan, G., and Harris, E., Evaluation of Serological Markers in Serum, Filter Paper Blood Spots, and Saliva for Dengue Diagnosis and Epidemiological Studies. Manuscript in preparation.

Baselt, D., Lee, G.U., Natesan, M., Metzger, S.W., Sheehan, P.E., and Colton, R.J., 1998. A biosensor based on magnetoresistance technology. Biosens. Bioelectron. 13, 731.

Besse, P-A., Boero, G., Demierre, M., Pott, V., and Popovic, R. S., 2002. Detection of a single magnetic microbead using a miniaturized silicon Hall sensor, App. Physics Let., 80, 4199.

Chemla, Y.L., Grossman, H.L., Poon, Y., McDermott, R., Stevens, R., Alper, M.D., and Clarke, J. 2000. Ultrasensitive magnetic biosensor for homogeneous immunoassay. Proc. Nat. Acad. Sci. 97, 14268.

Edelstein , R.L., Tamanaha, C.R., Sheehan ,P.E., Miller, M.M., Baselt, D.R., Whitman, L.J., and Colton,R.J., 2000. The BARC biosensor applied to the detection of biological warfare agents. Biosens. Bioelectron. 14, 805.

Erturk, M., Anna, R., Newton, K.M., Xia, T., Clark, W.F., 2006. BSIM Model for MOSFET Flicker Noise Statistics: Technology Scaling, Area, and Bias Dependence. Proc. NSTI Nanotech. Conf., 2006.

Fannin, P.C., Cohen-Tannoudji, L., Bertrand, E., Giannitsis, A.T., Mac Oireachtaigh, C., Bibette, J., 2006. Investigation of the complex susceptibility of magnetic beads containing maghemite nanoparticles. J. Magn. Magn. Mater. 303, 147.

Gehring, A.G., Irwin, P.L., Reed, S.A., Tu, S.I., Andreotti, P.E., Akhavan-Tafti, H., and Handley, R.S., 2004. Enzyme-linked immunomagnetic chemiluminescent detection of Escherichia coli O157:H7. J. Immunol. Methods 293, 97.

Gijs, M.A.M., 2004. Magnetic Bead Handing on-chip: new opportunities for analytical applications. Microfluid. Nanofluid. 1, 22.

Gundersen, S.G., Haagensen, I., Jonassen, T.O., Figenschau, K.J., de Jonge, N., and Deelder, A.M., 1992. Magnetic bead antigen capture enzyme-linked immunoassay in microtitre trays for rapid detection of schistosomal circulating anodic antigen. J. Immunol. Methods 148, 1.

Herne, T.M. and M. J. Tarlov. 1997. Characterization of DNA probes immobilized on gold surfaces. J. Am. Chem. Soc. 119, 8916.

Kurlyandskaya, G., and Levit, V., 2005. Magnetic Dynabeads detection by sensitive element based on giant magnetoimpedance. Biosens. Bioelectron. 20, 1611.

Lee, G.U., Metzger, S., Natesan, M., Yanavich, C., and Dufrene, Y.F., 2000. Implementation of force differentiation in the immunoassay. Anal. Biochem. 287, 261.

Mabey, D., Peeling, R.W., Ustianowski, A., and Perkins, M.D., 2004. Diagnostics for the Developing World. Nat. Rev. Microbiol. 2, 231.

Rife, J. C., Miller, M. M. , Sheehan, P. E. , Tamanaha, C. R. , Tondra, M. , and Whitman, L. J., 2003. Design and performance of GMR sensors for the detection of magnetic microbeads in biosensors. Sens. Actuators A 107, 209.

Safarik, I., and Safarikova, M., 2004. Magnetic techniques for the isolation and purification of proteins and peptides. Biomagn. Res. Technol. 2, 7.

Song, J.M., Culha, M., Kasili, P.M., Griffin, G.D., and Vo-Dinh, T., 2005. A compact CMOS biochip immunosensor towards the detection of a single bacteria. Biosens. and Bioelectron. 20, 2203.

Tondra, M., Popple, A., Jander, A., Millen, R.L., Pekas, N. and Porter, M.D., 2005. Microfabricated tools for manipulation and analysis of magnetic microcarriers. J. Magn. Magn. Mater. 293, 725.

Appendix A

Post-Processing Steps

1. Coat host wafer with ~1-μm G-line photoresist on coat track. Do not bake
2. Quickly mount chiplets on host wafer
3. Bake 2 min at 90 °C
4. Using resist pen, protect pad area
5. Bake 1hr at 120 °C
6. Using LAM 2 REI (starting recipe is *kyle5x*), alternate between:
    a. 20 sec. at 850W
    b. 90 sec. 0W (for cooling)

    Repeat until Metal-2 is exposed (turns white). Typically this involves 12 iterations. Inspect after every 60s to 90s of etch time.
7. Inspect resist, strip and reapply as necessary
8. Al-etch at 50 °C for about 2 min.
    a. Visually inspect regularly. Sensor area turns red/green
9. Strip resist
    a. Heat beaker large enough for wafer with Baker PRS-3000 at about 90-100 °C
    b. Immerse wafer until chips release. Can gently help with Teflon tweezers
10. Rinse in DI 3x
11. Final rinse in methanol
12. Load chiplets into hard mask/holder
13. Load hard mask/holder in Veeco Evaporation System
    a. Deposit 7 nm Chrome
    b. Deposit 15 nm Gold

Appendix B

Matlab Code

Top-level function list:

cal3.m	(for calibration)
measure3.m	(for measurement)

Lower-level function list:

parse4x4.m
getSideband5.m
normalize4.m
getPercent2.m

cal3.m

```
function B=cal(root_file,NUM_CALS,TIME)
%root_file is the root name string
%num_cals is the number of cal cycles
%returns array CalData

ARRAY_SIZE=1024;
ERROR=0;
ERROR_MAX=1 + floor(NUM_CALS/4);
M_CAL_THRESH=0.060;

%premake array
CData=zeros(NUM_CALS,ARRAY_SIZE);
error_cnt=0;

%initial power settings
old_power_setting=92;
refsigs=50;

fprintf('\n Calibration Round: \n');
for j=1:NUM_CALS,
    fprintf('%d ',j);
   %create cal file string
   cal_filename=strcat(root_file,'_cal_',num2str(j),'.wav');

   %delete existing file
DELETE_STRING=strcat('del C:\MATLAB7\work\',cal_filename);

   %acquire recording
   flag=1;
   while ((flag==1)&&(ERROR==0))

[R,new_power_setting]=playRec3(cal_filename,TIME,refsigs,old_power_sett
ing);
       %read in filename
       y=wavread(cal_filename);
       diff_y= y(:,1)-y(:,2);

       %parse
       [dataY,pflag]=parse4x4(diff_y);
       %get signal
       dataS=getSideband5(dataY);
       %normalize for magnetic excitation
       clear tempData;
       [tempData,nflag,meanrefsigs]=normalize4(dataS);
       flag=nflag||pflag;


       %add to error count
       if (flag==1),
           error_cnt=error_cnt+1;
           %check if error count exceeds max
           if (error_cnt>ERROR_MAX)
               ERROR=1;
           end
```

```
        end
    end
    %lock in meanrefsigs
    refsigs=meanrefsigs
    old_power_setting=new_power_setting;
    %delete record file
   DELETE_STRING=strcat('del C:\MATLAB7\work\',cal_filename);
   dos(DELETE_STRING);
    if (ERROR==0)
        CData(j,1:length(tempData))=tempData;
    end
end
if (ERROR==0)
    CalData=CData(1:NUM_CALS,1:length(tempData));
    MCalData=mean(CalData);
    %check for any zeros
    if (all(CalData))
        display('valid Cal');
        % get mean and std for cal
        for j=2:NUM_CALS,
            mean_cal(j)=mean(abs(CalData(j,:)-mean(CalData)));
            std_cal(j)=std(abs(CalData(j,:)-mean(CalData)));
        end
        M_Cal=mean(mean_cal);
        S_Cal=mean(std_cal);
        fprintf('M_Cal: %f, S_Cal: %f \n',M_Cal,S_Cal);
        %save as .mat file
        mat_filename=strcat(root_file,'_cal_',num2str(TIME),'.mat');
        save(mat_filename,'CalData');
    end
else
display('INVALID CAL');
   ERROR=1;
    M_Cal=1000;
   S_Cal=1000;
end
B=[M_Cal,S_Cal,ERROR];
```

measure3.m

```
function PcentData=meas(root_file,NUM_MEAS,TIME,TIME2)
%root_file is the root name string

%returns array MeasData
%premake array
ARRAY_SIZE=1024;
%premake array
MData=zeros(NUM_MEAS,ARRAY_SIZE);

%initial power settings
old_power_setting=92;
refsigs=50;

fprintf('\n Measurement Round: \n');
for j=1:NUM_MEAS,
        fprintf('%d ',j);
   %create cal file string
   meas_filename=strcat(root_file,'_meas_',num2str(j),'.wav');

   %delete existing file
   DELETE_STRING=strcat('del C:\MATLAB7\work\',meas_filename);

   %acquire recording
   pflag=1;
   nflag=1;
   while ((pflag==1)||(nflag==1))

[R,new_power_setting]=playRec3(meas_filename,TIME,refsigs,old_power_set
ting);

        %read in filename
        y=wavread(meas_filename);
        diff_y= y(:,1)-y(:,2);

        %parse
        [dataY,pflag]=parse4x4(diff_y);

        %get signal
        dataS=getSideband5(dataY);

        %normalize
        clear tempData;
        [tempData,nflag,meanrefsigs]=normalize4(dataS);
   end

   MData(j,1:length(tempData))=tempData;
   %lock in meanrefsigs
   refsigs=meanrefsigs;
   old_power_setting=new_power_setting;
   %delete record file
   DELETE_STRING=strcat('del C:\MATLAB7\work\',meas_filename);
   dos(DELETE_STRING);
end
MeasData=MData(1:NUM_MEAS,1:length(tempData));
```

```
%save meas as .mat file
mat_filename=strcat(root_file,'_meas_',num2str(TIME),'.mat');
save(mat_filename,'MeasData');
%load cal .mat file
mat_filename=strcat(root_file,'_cal_',num2str(TIME2),'.mat');
load(mat_filename);

%adjust length to fit measured data (allows for shorter measurements)
ScaledCalData=CalData(:,1:length(1:length(MeasData(1,:))));

%evaluate
PcentData = getPercent2(root_file,MeasData,ScaledCalData);
```

parse4x4.m

```
function [dataP,flag]=parse(data)

SAMPLE_WIDTH=5645;
WINDOW_WIDTH=8;
REAL_SAMPLE_WIDTH=5644.8;
HEADER=1500;
START=1;
THRESHOLD1=1e-3;
flag=0;

%first find max, then check power
index=10000;
short_data=data(1:200000);
%START=58300;
while ((START==1)&&(index<150000)),
   temp_mean=mean(abs(short_data(index:index+WINDOW_WIDTH)));
   if temp_mean<THRESHOLD1,
      START=index+20;
   end
   index=index+4;
end

if ((START<20000)||(START>100000)),
    flag=1;
    fprintf('\n START: %d  \n',START);
    fprintf('WARNING:PARSE ERROR \n');
end;

data=data(START:length(data));

%parse
NUM_ELEM=floor(length(data)/SAMPLE_WIDTH);

dataP=zeros(SAMPLE_WIDTH-HEADER,NUM_ELEM);

for i=0:NUM_ELEM-1;
   index=round(i*REAL_SAMPLE_WIDTH);
   dataP(:,i+1)=data(index+HEADER+1:index+SAMPLE_WIDTH);
end
```

getSideband5.m

```
function P = getSideband4(dataP);

DATA_LENGTH=length(dataP(:,1));
NUM_ELEMENTS=length(dataP(1,:));

FFT_LENGTH=4096;
NUM_FFTS=floor(DATA_LENGTH/FFT_LENGTH);
f1=1299;
f2=1675;

FFT_WINDOW=hamming(FFT_LENGTH);
P=zeros(1,NUM_ELEMENTS);

for i=1:NUM_ELEMENTS, %OUTER LOOP FOR EACH ARRAY ELEMENT
   index=1;
   for j=1:NUM_FFTS, %PERFORM MULTIPLE FFTS ON EACH SAMPLE
      tempFFT=abs(fft(FFT_WINDOW.*dataP(index:index+FFT_LENGTH-
1,i),FFT_LENGTH));
      index=index+FFT_LENGTH;
      P(i)=(P(i)+tempFFT(f1)+tempFFT(f2));
   end
end
```

normalize4.m

```
function [norm_data,flag,meanRefSigs] = normalize (data);

NUM_REF_SIGS= floor(length(data)/32);
LEGACY_CONSTANT=60; %should be set to average of RefSigs for current
setup

%detect number of reference signals
flag=0;

%check that all ref sigs are in position
MIN_MEAN=20;
MAX_STD=1;
for k=1:NUM_REF_SIGS,
    tempRefSigs(k)=data(((k-1)*32)+1);
end
meanRefSigs=mean(tempRefSigs)
stdRefSigs=std(tempRefSigs);

if((meanRefSigs<MIN_MEAN)||(stdRefSigs>MAX_STD)),
    flag=1;
    fprintf('\nMean Ref Sigs: %f \n',meanRefSigs);
    fprintf('\nStd Ref sigs: %f \n', stdRefSigs);
    display('WARNING: REF SIGNAL ERROR (1)')
end

%Divide 31 values in between ref values by mean of RefSigs,multiply by
%LEGACY
norm_data=ones(NUM_REF_SIGS*31,1);
for j=1:NUM_REF_SIGS,
   index=(j-1)*32+2; %data index
   index2=(j-1)*31+1; %norm_data index

norm_data(index2:index2+30)=(data(index:index+30)/meanRefSigs)*LEGACY_C
ONSTANT;
end

%check for clock skip
if max(norm_data)>5,
    flag=1;
    display('WARNING: CLOCK SKIP')
    %max(norm_data)
end
norm_data=norm_data';
```

getPercent2.m

```
function P=getPercent(root_file,MeasData,CalData);

%MeasData is the measure data (N x M)
%CalData is the cal data (N x M)
NUM_CALS=length(CalData(:,1));
NUM_ELEM=length(CalData(1,:));

%Set threshold
THRESHOLD=0.045;

%evaluate measured data
MeasDelta=mean(MeasData(2:NUM_CALS,1:NUM_ELEM))-
mean(CalData(2:NUM_CALS,1:NUM_ELEM));

%get number of positives
count=0;
for k=1:length(MeasDelta),
   if abs(MeasDelta(k))>THRESHOLD,
      count=count+1;
   end
end
Pcent = count/length(MeasDelta);
M_meas=mean(abs(MeasDelta));
S_meas=std(abs(MeasDelta));
P=[M_meas,S_meas,Pcent];

bar(abs(MeasDelta),'k');
title(sprintf('Sample: %s   Percent: %3.2f',root_file,P(3)*100));
%title(1,'Percent: %3.2f',Pcent*100);
fprintf('\n');
hold;
plot(THRESHOLD*ones(1,length(MeasDelta)),'r');
hold;
figure;
```

Appendix C

Purified-Protein ELISA Protocol

1. Add 100 µl of Fc-specific anti-mouse IgG (Jackson ImmunoResearch, West Grove, PA), diluted to 1.7 µg/ml in carbonate coating buffer (0.05 M carbonate/bicarbonate, pH 9.6), to wells of 96-well plate (MaxiSorp, Nalge Nunc International, Rochester, NY).
2. Incubate for 16 hr. at 4 °C.
3. Wash 1X with 150 ul PBS-T (PBS pH 7.3, 0.05% Tween-20).
4. Add 150 µl non-fat dry milk (NFDM) diluted to 3% in coating buffer
5. Incubate for 2 hr. at RT.
6. Wash 3X with 150 ul PBS-T.
7. Add 100 µl of purified mouse IgG (Jackson ImmunoResearch), diluted to 1 µg/ml, 100 ng/ml, 10 ng/ml, 1 ng/ml, and 100 pg/ml in PBS.
8. Incubate for 16 hr. at 4 °C.
9. Wash 3X with 150 ul PBS-T.
10. Add 100 µl of 0.2 µg/ml biotinylated Fab-specific goat anti-mouse IgG (Jackson ImmunoResearch).
11. Incubate 1 hr. at RT.
12. Wash 3X with 150 ul PBS-T.
13. Add 100 µl of 1.5-µg/ml streptavidin-alkaline phosphatase (AP) (Zymed Laboratories, San Francisco, CA).
14. Incubate for 1 hr. at RT.
15. Wash 5X with 150 ul PBS-T.
16. Add 100 µl of 1.5-mg/ml p-nitrophenyl phosphate (pNPP) in 0.2 M tris buffer (Sigma Chemical Co., St. Louis, MO).
17. Incubate in dark for 15 min. at RT.
18. Add 100 µl of 3 M NaOH.
19. Read plate using a 405-nm filter on ELx808 Microplate Reader (Bio-Tek Instruments Inc., Winooski, VT).

Appendix D

Purified-Protein MPA Protocol

1. Add 100 µl of Fc-specific anti-mouse IgG (Jackson ImmunoResearch, West Grove, PA), diluted to 1.7 µg/ml in carbonate coating buffer (0.05 M carbonate/bicarbonate, pH 9.6), to sensor module sample well.
2. Incubate for 16 hr. at 4 °C.
3. Wash 1X with 150 ul PBS-T (PBS pH 7.3, 0.05% Tween-20).
4. Add 150 µl non-fat dry milk (NFDM) diluted to 3% in coating buffer
5. Incubate for 2 hr. at RT.
6. Wash 3X with 150 ul PBS-T.
7. Add 100 µl of purified mouse IgG (Jackson ImmunoResearch), diluted to 1 µg/ml, 100 ng/ml, 10 ng/ml, 1 ng/ml, and 100 pg/ml in PBS.
8. Incubate for 16 hr. at 4 °C.
9. Wash 3X with 150 ul PBS-T.
10. Add 100 µl of 0.2 µg/ml biotinylated Fab-specific goat anti-mouse IgG (Jackson ImmunoResearch).
11. Incubate 1 hr. at RT.
12. Wash 3X with 150 ul PBS-T.
13. Add 150 µl of beads (2-20 µm, Polysciences Inc., Warrington, PA), diluted 1:100 to a concentration of 200 µg/ml. Vortex beads for 15 sec. before use.
14. Allow beads to settle for 15 min.
15. Place 5-mm barrel-type rare-earth magnet (ForceField, Fort Collins, CO) in contact with fluid for 30 sec.
16. Measure sample with reader system within 2 min. of magnetic washing.

Appendix E

Serum ELISA Protocol

1. Add 100 µl of dengue viral antigens (serotypes 1-4), prepared from lysed dengue virus-infected C6/36 mosquito cells (Balmaseda et al., 2003), diluted to 70 mg/ml in carbonate coating buffer (0.05 M carbonate/bicarbonate, pH 9.6), to wells of 96-well plate (MaxiSorp, Nalge Nunc International, Rochester, NY).
2. Incubate for 16 hr. at 4 °C.
3. Wash 1X with 150 ul PBS-T (PBS pH 7.3, 0.05% Tween-20).
4. Add 150 µl non-fat dry milk (NFDM) diluted to 3% in coating buffer
5. Incubate for 2 hr. at RT.
6. Wash 3X with 150 ul PBS-T.
7. Add 100 µl of human serum sample, diluted 1:100 in 3% NFDM/PBS.
8. Incubate for 12-18 hr. at 4 °C.
9. Wash 3X with 150 ul PBS-T.
10. Add 100 µl of 0.2 µg/ml biotinylated goat anti-human IgG polyclonal (Jackson ImmunoResearch).
11. Incubate 1 hr. at RT.
12. Wash 3X with 150 ul PBS-T.
13. Add 100 µl of 1.5-µg/ml streptavidin-alkaline phosphatase (AP) (Zymed Laboratories, San Francisco, CA).
14. Incubate for 1 hr. at RT.
15. Wash 5X with 150 ul PBS-T.
16. Add 100 µl of 1.5-mg/ml p-nitrophenyl phosphate (pNPP) in 0.2 M tris buffer (Sigma Chemical Co., St. Louis, MO).
17. Incubate in dark for 15 min. at RT.
18. Add 100 µl of 3 M NaOH.
19. Read plate using a 405-nm filter on ELx808 Microplate Reader (Bio-Tek Instruments Inc., Winooski, VT).

Appendix F

Serum MPA Protocol

1. Add 100 µl of dengue viral antigens (serotypes 1-4), prepared from lysed dengue virus-infected C6/36 mosquito cells (Balmaseda et al., 2003), diluted to 70 mg/ml in carbonate coating buffer (0.05 M carbonate/bicarbonate, pH 9.6), to sample well.
2. Incubate for 16 hr. at 4 °C.
3. Wash 1X with 150 ul PBS-T (PBS pH 7.3, 0.05% Tween-20).
4. Add 150 µl non-fat dry milk (NFDM) diluted to 3% in coating buffer
5. Incubate for 2 hr. at RT.
6. Wash 3X with 150 ul PBS-T.
7. Add 100 µl of human serum sample, diluted 1:100 in 3% NFDM/PBS.
8. Incubate for 12-18 hr. at 4 °C.
9. Wash 3X with 150 ul PBS-T.
10. Add 100 µl of 0.2 µg/ml biotinylated goat anti-human IgG polyclonal (Jackson ImmunoResearch).
11. Incubate 1 hr. at RT.
12. Wash 3X with 150 ul PBS-T.
13. Add 100 µl of 1.5-µg/ml streptavidin-alkaline phosphatase (AP) (Zymed Laboratories, San Francisco, CA).
14. Incubate for 1 hr. at RT.
15. Wash 5X with 150 ul PBS-T.
16. Add 150 µl of beads (4.1 µm, 1% w/v, Spherotech Inc., Libertyville, IL), diluted 1:20 in 0.3% NFDM/PBS. Vortex beads for 15 sec. before use.
17. Allow beads to settle for 30 min.
18. Connect magnetic-washing adapter to electromagnet and apply 460 Gauss/cm (approx. 2.5A) for 30 sec.
19. Remove adapter and measure sample with reader system within 2 min. of magnetic washing.